Observations of Europa's Tenuous Atmosphere

M. A. McGrath
NASA Marshall Space Flight Center

C. J. Hansen and A. R. Hendrix
NASA Jet Propulsion Laboratory/California Institute of Technology

Europa is known to possess a predominantly molecular oxygen atmosphere produced by sputtering of its icy surface. This atmosphere, which is diagnostic of surface composition and processes, has been characterized by the Hubble Space Telescope, Galileo, Cassini, and ground-based observations. The primary means of detecting Europa's atmosphere is via emission from the atomic constituents. The relative strengths of the atomic oxygen emission lines allow inference of a dominant O_2 component. Oxygen, sodium, and potassium are the minor constituents detected to date. An ionosphere has also been detected on several occasions by Galileo radio occultation measurements, the presence of which appears to require a sunlit, plasma bombarded (trailing) hemisphere. Neither the spatial distribution of the oxygen emission associated with the atmosphere, nor the obvious variability of the atmospheric emissions and the ionospheric densities, has been adequately explained to date.

1. INTRODUCTION

Europa is one of a growing cadre of solar system objects that possess tenuous atmospheres. Their discovery — at Mercury, the Moon, Io, Europa, Ganymede, Callisto, Enceladus, Triton, and Pluto — has become common in recent years because of the increasing sophistication of remote sensing and *in situ* observing techniques. They are produced by a wide variety of physical processes, including sublimation, sputtering (by both photons and charged particles), micrometeroid bombardment, geysers, and volcanos. This class of atmosphere is important because of the often unique information these atmospheres can provide about the surrounding environment (which also has implications for understanding the magnetospheres of the parent planets), surface processes, and therefore, potentially, interior and surface compositions of these bodies. Although tenuous, these exospheres also produce measurable ionospheres with peak densities of ~10^3–10^4 cm^{-3}, which were one of the first definite indications of the presence of atmospheres associated with these bodies (e.g., *Kliore et al.,* 1974, 1975).

The idea that the Galilean satellites might possess tenuous atmospheres, and that satellites with atmospheres could possess neutral tori, began to be explored in earnest in the early 1970s with a series of important milestones. Water ice was positively identified on the surfaces of Europa, Ganymede, and Callisto by *Pilcher et al.* (1972). An approximately 1-μbar atmosphere was reported on Ganymede from a stellar occultation measurement (*Carlson et al.,* 1973). *McDonough and Brice* (1973) suggested that, as a consequence of their atmospheres, there might be neutral clouds of orbiting atoms associated with Titan and the Galilean satellites because most material removed from the atmospheres does not attain escape velocity from the planet. Detection of hydrogen (H) (*Judge and Carlson,* 1974), sodium (Na) (*Brown,* 1974), and potassium (K) (*Trafton,* 1975) clouds associated with Io seemed to confirm these early expectations. Pioneer 10 observations of Europa made in 1973 using the long wavelength channel ($\lambda < 1400$ Å) of the ultraviolet (UV) photometer were first reported as a null result (*Judge et al.,* 1976), but subsequently reported as a detection of oxygen (O) at Europa using the short wavelength ($\lambda <$ 800 Å) UV photometer channel (*Wu et al.,* 1978). Around this time the Io plasma environment also began to be characterized (*Frank et al.,* 1976; *Kupo et al.,* 1976). The realization that Europa, like Io, is immersed in and impacted by a high flux of particles that could dissociate and sputter water ice (*Brown et al.,* 1977) made the possibility of a tenuous atmosphere and extended neutral clouds associated with Europa seem much more plausible.

The *Carlson et al.* (1973) detection motivated *Yung and McElroy* (1977) to develop a photochemical model of a sublimation-driven water ice atmosphere. Because the H preferentially escapes, such an atmosphere evolves into a stable molecular oxygen atmosphere by photolysis of H_2O. In their model, nonthermal escape of O atoms balances the production of O_2 to yield a surface pressure of ~1 μbar, consistent with the *Carlson et al.* (1973) result. They concluded that Ganymede should have an appreciable oxygen atmosphere and ionosphere, but that the higher albedo of Europa would inhibit sublimation, suppressing the formation of O_2. Based on laboratory data, *Lanzerotti et al.* (1978) suggested that bombardment of the satellite surfaces by the jovian plasma leads to an erosion rate on Ganymede that could support the H_2O partial pressure used by *Yung and McElroy* (1977), and that the rates would be much larger at Europa. Subsequent laboratory data showed that O_2 is directly produced in and ejected from water ice (*Brown et*

al., 1980), a process referred to as radiolysis. When the Voyager 1 Ultraviolet Spectrometer stellar occultation measurements of Ganymede yielded an upper limit on surface pressure of 10^{-5} μbar (*Broadfoot et al.,* 1979), *Kumar* (1982) pointed out that the *Yung and McElroy* (1977) model possessed an additional stable solution with a much lower surface pressure of ~10^{-6} μbar, compatible with the Voyager 1 result.

Finally, using the laboratory sputtering data of *Brown et al.* (1980), *Johnson et al.* (1982) estimated that O_2 sputtered from water ice on Europa could yield a bound atmosphere with a column density of ~(2–3) × 10^{15} cm^{-2}. Since O_2 does not stick efficiently at Europa temperatures and does not escape efficiently, the atmosphere is dominated by O_2 even though the sputtered flux of H_2O molecules is larger than that of O_2. This early work set the stage for the successful detection of oxygen at Europa, which we describe in detail below.

Generally speaking, Europa's tenuous atmosphere is produced by radiolysis and sputtering of its icy surface, with a minor contribution from sublimation of water ice near the subsolar point. As pointed out by *Johnson* (2002), Europa is an example of a surface bounded atmosphere. Once products are liberated from the surface, the diatomic species (primarily O_2, but to a lesser extent H_2) are expected to become the dominant ones because they are noncondensable, neither sticking nor reacting efficiently with the surface and therefore accumulating in the atmosphere, but becoming thermalized through repeated surface encounters. The other water group species are lost either by direct escape because they are light, or by sticking to or reacting with the surface. A summary of the observations acquired to date pertinent to Europa's atmosphere is provided in Table 1. Figure 1 illustrates schematically the species detected, and the range of altitudes over which the detections have been made, where 1 Europa radius (R_E) is 1569 km. It is important to note that the various observations span quite different regimes of the atmosphere, neutral clouds, and torus. In particular, observations of the main constituent of the atmosphere, O_2, and observations of the minor species, Na and K, have no overlap. A rough boundary between the bound atmosphere and neutral clouds is the radius of the Hill sphere of Europa, which occurs at ~8.7 R_E. Inside this boundary, Europa's gravitational field dominates Jupiter's; outside this boundary the opposite is true. We discuss the various observations roughly in order of increasing distance from Europa's surface, considering first the bound O_2 atmosphere, which has a scale height of roughly ~100 km.

We concentrate in this chapter on providing detailed descriptions of the observations made to date of Europa's tenuous atmosphere. The subsequent chapter by Johnson et al. provides a complementary review of the detailed interpretations and modeling these observations have spawned. It includes an in-depth discussion of the wide range of physical characteristics that can be gleaned about Europa and its environment from these observations. We focus here on providing a clear explanation of the quality and limitations of the existing observations and data, and on providing descriptions of the simple models presented in the observational papers required to derive basic quantities such as column densities from the observations. Where possible we provide further details about and new presentations of previously published data. Finally, we summarize outstanding issues, and provide recommendations for future observations that may be helpful in resolving them.

2. OXYGEN ATMOSPHERE

The major constituent of Europa's tenuous atmosphere is now known to be molecular oxygen, which has been inferred via detection of UV line emission from atomic oxygen. Emission from neutral atmosphere constituents are overwhelmed by reflected sunlight at visible wavelengths, whereas at UV wavelengths most planetary bodies have albedos more than an order of magnitude lower than in the visible. Ten sets of ultraviolet observations of Europa now exist, seven made with the Earth-orbiting Hubble Space Telescope (HST), two made with the Cassini spacecraft, and one made with the New Horizons spacecraft. The specifics of the observations are summarized in Table 1. The HST and New Horizons observations acquired in February 2007 are not yet published but preliminary results have been presented by *Retherford et al.* (2007). The HST observations made in April 2007 and June 2008 are not yet published, and no results have been presented to date.

2.1. Hubble Space Telescope Observations

The first unambiguous detection of Europa's atmosphere was made by *Hall et al.* (1995) in June 1994 using HST's Goddard High Resolution Spectrograph (GHRS) with a 1.74" × 1.74" slit centered approximately on Europa's trailing hemisphere. They discovered emission from the semi-forbidden and optically allowed oxygen multiplets O I ($^5S^o$–^3P)1356 Å and O I ($^3S^o$–^3P)1304 Å (bottom panel of Fig. 2). In these and subsequent observations of the UV oxygen emission multiplets there are several possible contributors to the observed emissions:

(1) solar resonance fluorescence scattering by O atoms in the Earth's atmosphere (HST only)

(2) solar emission line and continuum photons reflected from the surface of Europa

(3) solar resonance fluorescence scattering by O atoms in Europa's atmosphere

(4) electron impact excitation of oxygen, $e^- + O \rightarrow O^* \rightarrow O + \gamma$

(5) electron impact dissociative excitation of O_2, $e^- + O_2 \rightarrow O^* \rightarrow O + \gamma$.

TABLE 1. Summary of Europa atmosphere observations.

Obs#	Date	Facility, Instrument	Range to Europa	Subobservation W Longitude, Orbital Phase	λ_{III}	Start (UT) Duration	Integration Time	Reference
Oxygen								
1	2 Jun 1994	HST GHRS	4.57 AU	283–318	156–53	09:52; 8 h 2 min	7290 s	*Hall et al.* (1995)
2	21 Jul 1996	HST GHRS	4.22 AU	85–108	317–139	08:43; 5.5 h	7398 s	*Hall et al.* (1998)
3	30 Jul 1996	HST GHRS	4.27 AU	264–287	280–99	04:59; 5.5 h	5549 s	*Hall et al.* (1998)
4	5 Oct 1999	HST STIS	4.01 AU	245–273	304–156	08:39; 7 h	9360 s	*McGrath et al.* (2004)
5	6 Jan 2001	Cassini UVIS	11.2 × 10^6 km	201–220, 290–311	159–277	7:30; 4.7 h	17000 s	*Hansen et al.* (2005)
6	12 Jan 2001	Cassini UVIS	15.8 × 10^6 km	64–103, 173–223	62–180–67	6:30; 11.4 h	41000 s	*Hansen et al.* (2005)
7	26 Feb–3 Mar 2007	New Horizons Alice	46.25–67.08 R_J	N/A	N/A	19:17; several days	6540 s	*Retherford et al.* (2007)
8	27 Feb 2007	HST ACS F125LP	5.42 AU	347–350 (eclipse)	94	12:03; 42 min	2400 s	*Retherford et al.* (2007)
9	18 Apr 2007	HST ACS PR130L	4.66 AU	343–352	296	04:34; 2.33 h	5200 s	unpublished; HST program #11085, P.I. W. Sparks
10	29 Jun 2008	HST ACS PR130L	4.18 AU	74–104	23–252	04:13; 7 h 9 min	12996 s	unpublished; HST program #11186, P.I. J. Saur
Ionosphere (radio occultations; N = entry, X = exit)								
11	19 Dec 1996	Galileo S band radio	1650 km, E4N	345, ~255	109	7:37	Not available	*Kliore et al.* (1997, 2001, 2006)
			4070 km, E4X	165, ~255		7:49		
12	20 Feb 1997	Galileo S band radio	1490 km, E6aN	280, ~192	298	17:56	Not available	*Kliore et al.* (1997, 2001, 2006)
			4388 km, E6aX	101, ~192		18:08		
13	25 Feb 1997	Galileo S band radio	2776996 km, E6bNX	55, ~335	99	15:18	Not available	*Kliore et al.* (1997, 2001, 2006)
			2776180 km, E6b	236, ~335		15:24		
14	1 Feb 1999	Galileo S band radio	Not available, E19N	Not available, ~144	240	~2:13	Not available	*Kliore et al.* (2006)
			Not available, E19X		Not available	Not available		
15	3 Jan 2000	Galileo S band radio	2531 km, E26N	122, not available			Not available	*Kliore et al.* (2001, 2006)
			1096 km, E26X	329, not available				
Minor Species, Neutral Clouds, Torus								
16	5 Jun 1995	Mt. Bigelow echelle	4.32 AU	91–113	71–247	4:11; 5.5 h	4.33 h	*Brown and Hill* (1996)
17	9 Sep 1998	Keck HIRES	3.97 AU	243–248	134–175	8:01; 1.27 h	1800 s each at 3 positions	*Brown* (2001)
18	28 Dec 1999	Keck HIRES	4.55 AU	98–114	332–93	4:28; 3.5 h	6 sets of scans	*Leblanc et al.* (2002, 2005)
19	28 Nov 2000	KPNO McMath	4.05 AU	285–288	253–28	3:14; ~1 h	1200 s	*Leblanc et al.* (2005)
20	29 Nov 2000	KPNO McMath	4.05 AU	42–46	59–91	6:53; ~1 h	3600 s	*Leblanc et al.* (2005)
21	30 Nov 2000	KPNO McMath	4.05 AU	125–130	333–7	2:40; 1 h	3600 s	*Leblanc et al.* (2005)
22	10 Jan 2001	Cassini ISS	~200 R_J	253 (in eclipse)	95	10:36; >60 m	15 3.2-s exposures	*Porco et al.* (2003)
								Cassidy et al. (2008)
23	1 Jan 2001	Cassini INCA	~140 R_J	N/A	N/A	22:00; 15 h	15 h	*Mauk et al.* (2003)
24	12–13 Feb 2001	Cassini UVIS	(4.21–4.32) × 10^7 km	N/A	N/A	6:08; 29 h 4 min	28 h	*Hansen et al.* (2005)

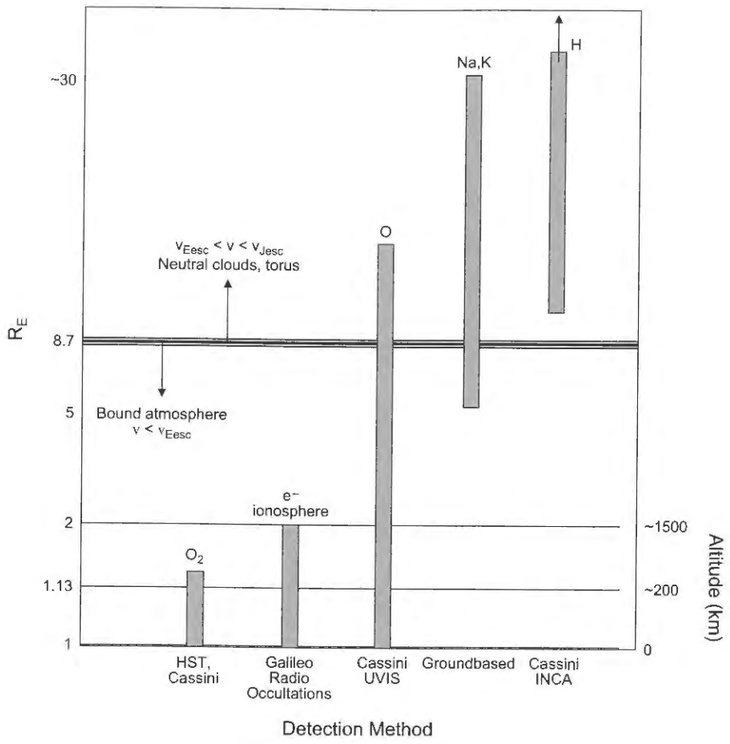

Fig. 1. Schematic diagram showing the constituents detected in Europa's tenuous atmosphere and the regions in which they have been observed. Generally speaking, the bound atmosphere is defined by the region within which Europa's gravity dominates, at $r \leq 8.7\ R_E$ ($1\ R_E = 1569$ km), where the velocity of the constituents is less than Europa's escape velocity (v_{Eesc}) of ~2 km/s. Beyond this region, particles either escape from Jupiter altogether ($v > v_{Jesc}$), or enter orbit around Jupiter as clouds or a torus near Europa's orbital distance.

The Hall et al. observations were performed in Earth shadow, where the contribution from process (1) is minimal; such background emission would fill the slit, and produce flat-topped emission line profiles, which was not observed. Figure 2 shows that in addition to the oxygen emissions, emission from C II 1335 Å is also detected; it is produced by process (2). Although the reflectivity with wavelength is unknown in the UV for Europa, if it is assumed to be constant with wavelength, the C II emission can be used to estimate the contribution to the oxygen emissions from process (2). Modeling the C II emission as reflected sunlight allows a derivation of the geometric albedo of Europa at this wavelength, which was found to be 1.6 ± 0.5% (*Hall et al.,* 1998). The contribution to the spectrum from process (2) is shown in Fig. 2 as a dark solid line underlying the observed spectrum. It is not a significant contributor to the O I 1356 Å emission line, which is a semiforbidden transition, because the Sun does not produce line emission at this wavelength. *Hall et al.* (1995, 1998) showed that process (3) produces a negligibly small contribution to the oxygen emissions at Europa.

The inference that process (5) dominates over process (4), and that Europa's atmosphere is predominantly O_2 and not O, is based on the ratio of the 1356 Å to 1304 Å emission intensities, I(1356)/I(1304). For the June 1994 observations, this ratio is ~1.9:1, after accounting for the contribution from processes (2) and (3). For a Maxwellian distribution of electrons over a broad temperature range this intensity ratio was found to be 2 for process (5) by *Noren et al.* (2001). By contrast, using the O I 1304 Å cross section of *Doering and Yang* (2001), the I(1356)/I(1304) ratio for process (4) has a broad maximum of 0.35 at 4 eV. A molecular oxygen atmosphere with column density 1.5 ± 10^{15} cm^{-2} ($P_o = 2.2 \pm 0.7 \times 10^{-6}$ μbar) was therefore inferred for the trailing hemisphere of Europa by *Hall et al.* (1995), which is consistent with the early estimate of a bound atmosphere by *Johnson et al.* (1982) and the low-pressure solution discussed by *Kumar* (1982). In deriving the O_2 column density, *Hall et al.* (1995) assumed that the spatial distribution of Europa's atmosphere is confined to the geometric cross section of the observed hemisphere (i.e., the scale height of the atmosphere is significantly smaller than the radius of Europa); a negligible contribution to the observed flux is emitted from above the tangential limb along the terminator; the Io plasma torus electrons responsible for exciting the observed emissions interact with the atmosphere without energy degradation; and no electrodynamic, sub-Alfvenic interactions such as observed by Voyager at Io (e.g., *Ness et al.,* 1979, *Neubauer,* 1980) were considered.

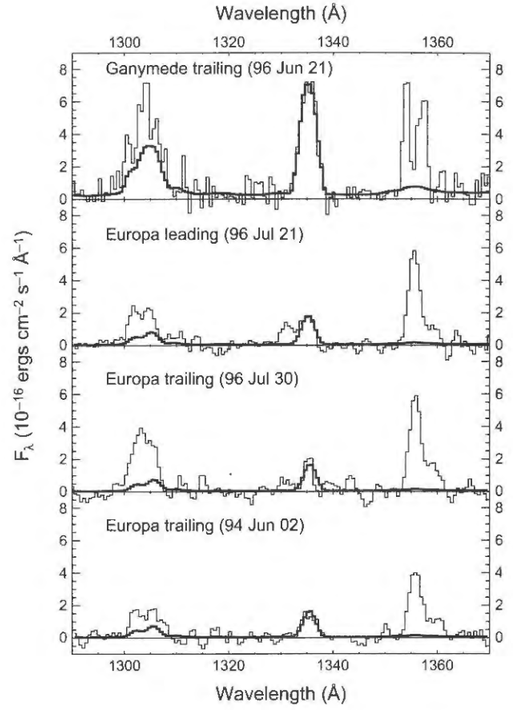

Fig. 2. The *Hall et al.* (1995, 1998) detections of electron excited oxygen emission at 1304 and 1356 Å from Europa, which provided the first direct evidence of an O_2 atmosphere on this satellite. The features at 1335 Å are due to solar C^+ emission reflected from the surface of the satellite. The dark line histogram shows a modeled reflected light spectrum that assumes the albedo is constant with wavelength, normalized by matching the 1335 Å feature. From *Hall et al.* (1998).

Two additional sets of GHRS observations were obtained in July 1996: one from the leading hemisphere, and an additional set from the trailing hemisphere (*Hall et al.,* 1998). All three of the GHRS spectra are shown in Fig. 2. With a finite scale height and emission above the limb included, the inferred molecular oxygen column densities are in the range ~$(2.4–14) \times 10^{14}$ cm^{-2}. Hall et al. noted that these observations were consistent with no atomic oxygen, and they set 3σ upper limits on the atomic oxygen abundances of $(1.6–3.4) \times 10^{13}$ cm^{-2}.

More recent cross-section work by *Kanik et al.* (2003) found that the emission ratio of 1356 to 1304 for process (5) ranges from ~2.5 to 3 for a Maxwellian distribution of T_e = 5 eV to ~2 to 2.5 for $T_e > 40$ eV. For the four sets of published HST observations (*Hall et al.*. 1998; *McGrath et al.,* 2004), the observed ratio varies from 1.3 ± 0.8 to 2.2 ± 1.4. The *Kanik et al.* (2003) cross section ratio therefore "does not support the Europa brightness observation for any energy." As noted by Kanik et al., this may imply that more atomic oxygen is present in Europa's atmosphere than deduced by *Hall et al.* (1998).

In 1999, observations of Europa's trailing hemisphere were obtained using the HST Space Telescope Imaging Spectrograph (STIS) with the 52" × 2" slit (the effective slit length is 25", determined by the size of the detector) and grating G140L, covering the wavelength range 1150–1720 Å (*McGrath et al.,* 2004). Two images were obtained in each of five HST orbits spanning 7 h, with the exception of the second exposure in the second orbit, which failed. Detailed information about the individual exposures is given in Table 1 of *Cassidy et al.* (2007). The data format, illustrated in Fig. 3, shows the type of information available in these observations: monochromatic images of Europa in emission lines of H I Lyman-α 1215.67 Å, O I 1304 Å, C II 1335 Å, and O I 1356 Å, as well as a disk-integrated spectrum of the satellite, which is directly comparable to the previous GHRS and subsequent Cassini observations.

Figure 4 shows the summed, monochromatic images at H I Lyman-α and oxygen wavelengths, as well as a representative visible light image of the corresponding hemisphere of Europa. The H I Lyman-α and O I 1304 Å images have had the geocoronal background (process (1)) subtracted off. The Europa signal in the Lyman-α image consists of solar Lyman-α photons reflected from the surface of the satellite (process (2)). The 1304 Å image consists of both emission from Europa's oxygen atmosphere (processes (4) and (5)), and solar 1304 Å oxygen emission reflected from the surface of Europa (process (2)), which is difficult to subtract from an image due to its unknown spatial distribution. As shown in Fig. 2, and discussed later in section 2.2 with regard to Cassini observations, the contribution of reflected light at 1304 Å does not dominate, but is nonneglibible. By contrast, the reflected component at 1356 Å is negligible because the Sun does not produce O I 1356 Å line emission, so this image includes only emission from the atmosphere of Europa. The O I 1356 image shown in Fig. 4 has a signal to noise ratio (S/N) of only ~3 in the brightest regions, and the O I 1356 Å emission peaks within the disk, not in a ring of emission at the limb of the satellite, as would be expected from plasma interaction with an optically thin atmosphere. It does display the expected limb glow (more easily seen in the middle panel of Fig. 3), but includes a brighter region within the disk on the antijovian hemisphere. Prior to the acquisition of these images, *Saur et al.* (1998) published a detailed model of the plasma in-

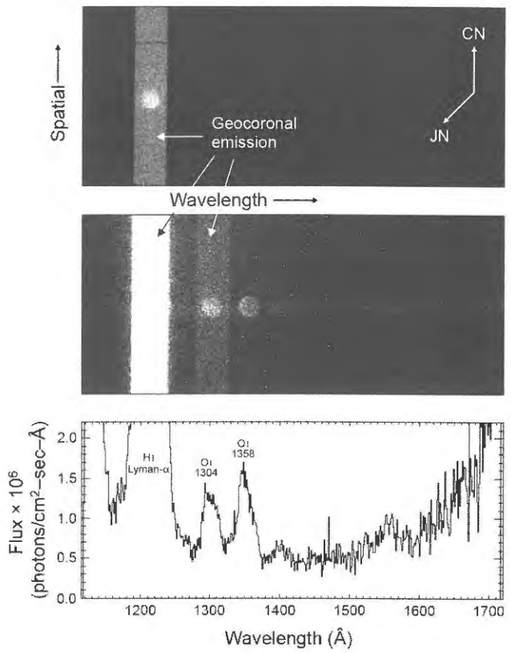

Fig. 3. Observation of Europa obtained in 1999 using the HST STIS, illustrating the data format. The top and middle panels are identical data displayed with a different stretch to emphasize Europa at H I Lyman-α wavelength (top) vs. the oxygen emissions (middle). Emission filling the long slit at H I Lyman-α and O I 1304 is from process (1). The one-dimensional spectrum in the bottom panel is obtained by summing over the spatial rows corresponding to Europa in the middle panel. CN = celestial north; JN = jovian (and Europa) north.

teraction at Europa, including a prediction of the morphology of the O I 1356 Å emission. Their prediction compared with the observation is shown in Fig. 19.10 of *McGrath et al.* (2004); the predictiou shows the brightest region off the limb of the subjovian hemisphere (opposite of that observed) and near the equator.

The observed brightness is an integral along the line of sight of the neutral density, the electron density, and an electron temperature dependent excitation rate coefficient. A localized bright region has to be caused by either nonuniform plasma effects (n_e, T_e) exciting the emissions, or nonuniform density of the sputtered neutral gas. It is difficult to understand why the brightest region is on the disk because of the reduced path length there. Since Europa has a weak induced magnetic field (*Kivelson et al.,* 1997) it seems unlikely that it could focus jovian electrons or energetic ions with finite gyro radii to sputter molecules into localized regions. The observation of localized O emission may suggest that the surface is not icy everywhere, but rather that the composition varies considerably with longitude, consistent with visible images and compositional data from Galileo. Comparison of the 1356 Å and visible images shows that the 1356 Å brightness may be correlated with the visibly brighter regions, which are thought to be purer water ice than the visibly darker regions. However, a preliminary analysis of the April 2007 HST observations does not support this hypothesis.

Cassidy et al. (2007) have explored the possibility of nonuniform sticking of O_2 as an explanation for the emission morphology. One caution concerning this interpretation is that the long integration time for the summed images shown in Fig. 4 limits the ability to distinguish between the possibilities of a spatially variable source/loss process or local variability of the plasma exciting the emission. The integration spans 7 h, over more than half of a Jupiter rotation, during which time local plasma conditions, and therefore the emission morphology, might be expected to change significantly due to the undulation of the plasma sheet associated with the tilted jovian magnetic field. In fact, although the region of the surface observed does not change significantly over the 7-h duration of the observations, the emission morphology does appear to vary, as shown in Fig. 5 where the individual images that were summed to produce the Fig. 4 image are shown. Unfortunately, these images have a very low S/N ratio of only ~1 in the brightest regions, so caution is needed to avoid overinterpretation. However, if the variation is real, it would tend to argue against interpretation of the bright region on the anti-Jupiter hemisphere as being associated with the corresponding bright visible region on the surface. Figure 5 shows that the brightest emission is always in the antijovian hemisphere, even though it appears to vary in latitude from north to south between images. As noted by *McGrath et al.* (2000) and *Ballester et al.* (2007), there is not a straightforward correlation between

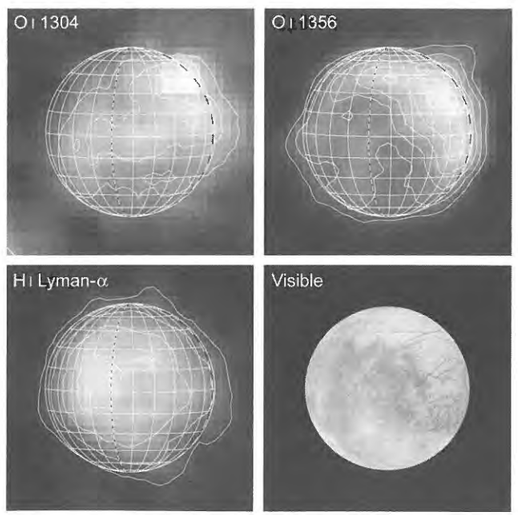

Fig. 4. O I 1304 Å, O I 1356 Å, and H I Lyman-α images from the HST observation shown in Fig. 3, along with a visible light image of the corresponding hemisphere of Europa.

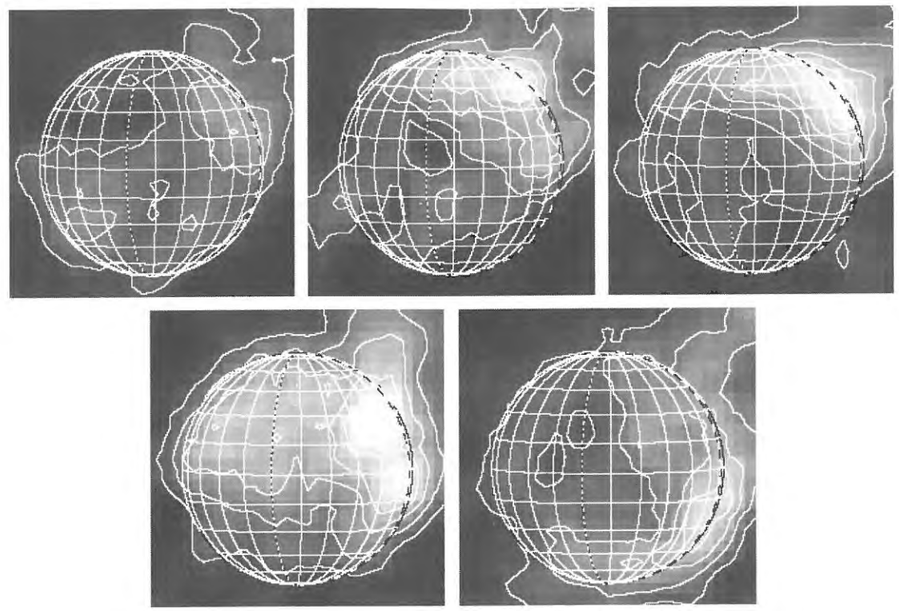

Fig. 5. O I 1356 images (shown with the same stretch) obtained in five consecutive HST orbits on October 5, 1999, over a time period of 7 h. These images were summed to produce the single O I 1356 image shown in Fig. 4. The S/N ratio in these images is only ~1 in the brightest regions. Care is therefore needed to avoid overinterpretation of the spatial and/or temporal variability that is obvious in these images.

the variation in emission location and the orientation of the hackground jovian magnetic field, as is the case for similar plasma excited emissions on Io.

Simple inspection of the images shown in Fig. 4 reveals an apparent correlation between the Lyman-α bright regions and the dark visible regions. This is likely due to surface albedo variations. The bright visible regions are thought to be composed of purer water ice, which is very dark at UV wavelengths, darker than most non-ice species (*Hendrix and Hansen,* 2008), so it is expected that more Lyman-α is reflected from the surface in the visibly darker surface regions than in the visibly brighter regions. A hydrogen corona such as that detected at Ganymede (*Barth et al.,* 1997; *Feldman et al.,* 2000) has been searched for in the Lyman-α images. It may be marginally present, but not with enough statistical significance to publish (K. D. Retherford, personal communication, 2008).

Four additional sets of UV observations of Europa exist (observations #7, 8, 9, and 10 in Table 1) but have not yet been published, although preliminary results for two of them (#7 and 8 in Table 1) have been presented in an oral talk at the December 2007 American Geophysical Union meeting (*Retherford et al.,* 2007). HST observations were made in February 2007 in conjunction with the New Horizons fly by of Jupiter, during which the New Horizons Alice instrument was also used to observe Europa. The Alice observations produced 17 spectra of Europa in sunlight from ~1250 to 1500 Å, 8 of which provided adequate signal for atmospheric emission measurements. The O I 1304 Å emission is barely detected in the composite spectrum. The brightness ratio of the 1356 Å to 1304 Å emissions is close to 2, as for previous HST observations, implying an O_2 source. There are no obvious trends vs. time in these spectra. Alice observations of Europa in eclipse failed. The accompauying HST observations were done with the Advanced Camera for Surveys (ACS) using the solar blind channel and filter F125LP to acquire 4 10-min exposures while Europa was in eclipse (observation #7 in Tahle 1), covering the subjovian hemisphere and Europa's magnetospheric wake, as opposed to the trailing (upstream) hemisphere of the satellite captured previously (shown in Figs. 4 and 5). Most of the signal in these images is due to detector dark noise, and because Europa is in eclipse, the location of the Europa disk is uncertain. There is a faint enhancement in emission above the background in these images. Retherford et al. have done limb fits to this faint emission to determine the location of the satellite, which they surmise is located 1.4" from the Fine Guidance Sensor determined pointing, larger than the nominal 1" pointing uncertainty. With this limb fit, they have produced an image that shows a bright region on the disk at northern latitude in the subjovian hemisphere, and an extended bright region extending off the disk that they interpret as wake emission. Wake emission would be surprising because it is expected that Europa's wake would have the lowest electron temperatures and densities of any region near Europa (*Kliore et al.,*

1997; *Saur et al.*, 1998; *Schilling et al.*, 2008). If this interpretation is correct, it tends to further support interpretation of the UV emission morphology as due to plasma, and not surface, effects.

The two additional unpublished sets of HST observations were made using the HST ACS with the prism, PR130L, in April 2007 and June 2008. The April 2007 set (#9 in Table 1) acquired two exposures in sunlight prior to Europa entering eclipse, and two exposures in eclipse. Ultraviolet emission at 1304 Å and 1356 Å is detected above the background in the sunlit images. The two eclipse images also show emission above background, presumably from oxygen at 1356 Å, although its location relative to the Europa disk is uncertain. The detected emission appears to be on the subjovian hemisphere at the limb of the satellite, very similar to the Cassini Na emission images discussed in section 4.1 and shown in Fig. 12. The June 2008 observations (#10 in Table 1) used the same setup as observation set #9 but of the leading hemisphere of Europa in sunlight. These data are still proprietary, with no results yet available.

2.2. Cassini Observations

Observations of the Galilean satellites were acquired by the Cassini spacecraft in December 2000 and January 2001 when it flew by Jupiter on the way to its primary orbital mission at Saturn. Much of the best satellite data were lost when the spacecraft entered safe mode a week before closest approach, however, two UltraViolet Imaging Spectrograph (UVIS) observations of Europa were acquired in the week following closest approach. The objective of these observations was to confirm the *Hall et al.* (1995) detection of a tenuous oxygen atmosphere and to compare these data, acquired at different times and for different orbital geometries, to the HST results.

Europa data pertinent to the atmosphere were acquired with the UVIS far-ultraviolet (FUV) channel (1115–1914 Å) on January 6 and 12, 2001. Details about the observations are given in Table 1. Further details, including graphical representations of the slit orientations for the two observing dates, are given in Table 1 and Fig. 1 of *Hansen et al.* (2005). The UVIS, like the HST STIS, has a two-dimensional detector that collects up to 1024 spectral pixels and 64 spatial pixels. For the Europa observations, the spatial pixels subtended 1.0 mrad, and the spectral pixels 0.25 mrad, while the slit width was 1.5 mrad. Europa subtended 0.28 mrad on January 6, and 0.20 mrad on January 12, meaning it was essentially a point source in both the spatial and spectral dimensions for both observations. Because Europa was boresighted for the Cassini ISS camera, and the FUV channel is offset 0.37 mrad from the ISS boresight, Europa was not centered in the slit for the observations, which results in a slight wavelength shift of the emission lines in the spectral direction, and causes Europa to span spatial rows 31 and 32 in both observations. The total duration of the January 6 observation was 17,000 s, in 17 1000-s integrations, while the January 12 observation collected 41 1000-s images. The observation geometries from Cassini were quite different than the view available to Earth-based telescopes because Europa was observed at greater than 90° phase angle, and portions of both the leading and trailing hemispheres, and sunlit and night sides, of Europa were included on both observing dates. The UVIS slit was oriented perpendicular to Jupiter's equatorial plane for both observations. On January 6 Europa was on the nightside of Jupiter in its orbit, while on January 12 it was on the dayside of Jupiter, near the ansa of its orbit as seen from Cassini, and it was tracked from the farside of its orbit, around the ansa to the nearside over the duration of the observation.

The nonoxygen emissions present in the full spectrum were from the Io plasma torus. The individual lines of the 1304 Å triplet at 1302.2, 1304.9, and 1306.0 Å and the 1356 Å doublet at 1355.6 and 1358.5 Å were all resolved in the UVIS spectrum, consistent with observation of a point source in the spectral direction, as noted above. The 1335 Å feature was used to determine an albedo of ~1% at 94° phase angle (compared with values of 1.3–1.6% from the HST observations), and account for the reflected solar light contribution to Europa's spectrum at 1216, 1304, and 1356 Å, assuming the albedo is flat throughout this region of the spectrum. Subtraction of the reflected light leaves the signal due solely to Europa's atmosphere. Since Europa was well away from the Io torus at the time of the January 12 observation there were no torus emissions to remove from the spectra. Atomic and molecular oxygen abundances derived from Cassini data are tabulated in Table 3. These are derived values, based on the flux observed at the instrument. Assumptions that go into these derived values include the scale height of the atmosphere, and the electron energy and density. *Hall et al.* (1998) derived a molecular oxygen vertical column density of $(2.4–14) \times 10^{14}$ cm^{-2}. Cassini molecular oxygen abundances fall within this range. The error bars on the Cassini measurements are ±~15%.

A point source provides the best fit to the shape of the 1356 Å emission feature, consistent with a bound, near-surface O_2 atmosphere with scale height of ~200 km (assuming a temperature of 1000 K). Once the 1356 Å feature was fit, the abundance of molecular oxygen and its contribution to the 1304 Å feature could be calculated. The remaining flux at 1304 Å was then attributed to the resonant scattering of sunlight by atomic oxygen (process (3)), and electron excitation of atomic oxygen (process (4)). Although somewhat subjective, the spectrum was best fit by including ~2% atomic O in the (point source) bound O_2 atmosphere, plus an extended tenuous atomic oxygen component overfilling a pixel. *Hall et al.* (1995, 1998) would not have been able to identify an extended O component, since Europa filled most of the field of view of the GHRS slit, whereas Europa subtends less than one spatial pixel in the UVIS slit, thus more of the surrounding space is measured, enabling the UVIS detection of the extended atomic oxygen component.

The spatial capability of UVIS was used to determine the oxygen profile as a function of distance from Europa. Figure 6a shows the distribution of oxygen in the January 6 dataset and Fig. 6b the January 12 dataset as a function of spatial row. An extended oxygen component is apparent in both sets of observations. The 1356 Å feature is sharply peaked at row 32. The diffuse 1304 Å feature persists across all the illuminated spectral pixels and is detectable in rows 28, 29, and 30. Although the low spatial resolution prevents determination of the size of the diffuse extended atmosphere, and any potential asymmetries such as suggested by *Burger and Johnson* (2004) for Europa's Na cloud, the atomic oxygen cloud appears to be about one pixel in extent, or ~11,000 km (~7 R_E) at Cassini's range. The density of oxygen in Europa's extended atmosphere is estimated to be roughly 1700 (January 6) and 1000 (January 12) atoms cm^{-3}, which was calculated using the simple formula (intensity in rayleighs × 10^6)/(pathlength in cm × probability of emission) where the probability of emission (combination for 1302 + 1304 + 1306) is 6.05×10^7 and the pathlength is assumed to be 22,000 km. This detection of atomic oxygen as an extended atmosphere adds a new observational constraint to models of the erosion of Europa's surface and the life cycle of its atmosphere in the jovian environment, such as those developed by *Saur et al.* (1998), *Shematovich and Johnson* (2001), and *Shematovich et al.* (2005).

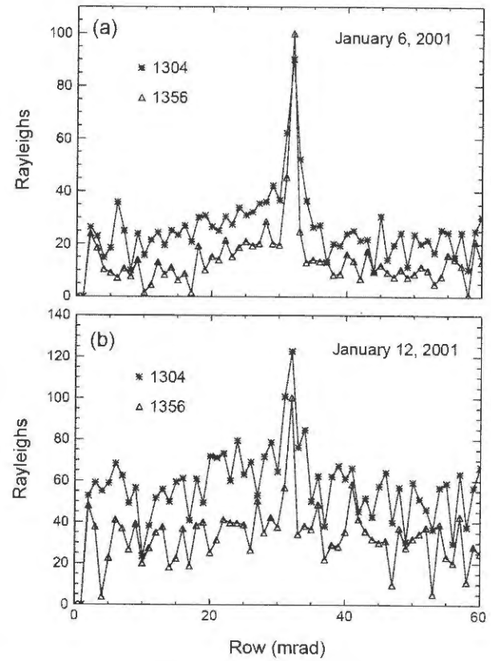

Fig. 6. The distribution of 1304 Å and 1356 Å oxygen emission along the slit in the spatial direction. **(a)** In the January 6, 2001, data the 1356 Å feature is sharply peaked at the position of Europa, while the diffuse 1304 Å feature source persists across all the illuminated spectral pixels; it is detectable in row 28, which corresponds to tbe opposite side of Europa's orbit, and then gradually drops to the background level. **(b)** The oxygen line emissions for the January 12, 2001, data. Most of these data were collected near the ansa of Europa's orbit as seen from Cassini. Both 1304 Å and 1356 Å are sharply peaked at Europa's position.

3. IONOSPHERE

In simple terms, an ionosphere is a layer of plasma produced by photo- and/or particle-impact ionization of a neutral atmosphere. In deep space planetary missions, ionospheres are detected by transmitting a one (or two)-way radio signal from the spacecraft to Earth (and back) through the atmosphere of the object of interest along a trajectory that produces an occultation of the spacecraft as seen from Earth. Such an occultation produces both an inbound and an outbound measurement of the target's ionosphere. In these radio occultations, a time series of signal strength and frequency are produced, and via comparison with a time series of predicted frequency computed from a precise spacecraft ephemeris, a set of frequency residuals is derived. The residuals are inverted using standard techniques to obtain the refractivity, which is directly related to electron density, thereby providing an electron density profile vs. altitude above the surface of the object.

The Galileo mission provided four radio occultations of Europa: one in orbit E4, two in orbit E6 (E6a and E6b), and one in orbit E26, as well as a near-occultation in orbit E19. The geometries and results from three of these (E4, E6a, and E6b) are shown in Figs. 1, 2, and 3 of *Kliore et al.* (1997). In addition, the E19 flyby resulted in detections on both the entry and exit paths, and the E26 fly resulted in a nondetection on the entry (designated by "N") leg, and a weak to nondetection on the exit (designated by "X") leg (*Kliore et al.*, 2001, 2006). The results of the 10 inbound and outbound measurements are shown in Fig. 7, and include six strong detections (E4N, E4X, E6aN, E6bN, E19N, E19X), one moderate to weak detection (E6bX), and three weak to nondetections (E6aX, E26N, E26X) of the ionosphere. [Note that the results shown in Fig. 7 and presented in *Kliore et al.* (2006) show lower electron densities and somewhat different profiles for E6b than those published in *Kliore et al.* (1997).] The maximum electron densities of ~10^3–10^4 cm^{-3} occur at or near the surface of Europa (except for E6bN, which peaks at ~100 km altitude) with a plasma scale height of ~200 km below 300 km, and ~400 km above 300 km altitude. Assuming likely candidate constituents such as H_2O, O_2, H, H_2, OH, and O leads to an estimated neutral density on the order of 10^8 cm^{-3}, and a column density on the order of 10^{15} cm^{-2} assuming a neutral scale height of ~100 km.

The E4N detection geometry is looking toward the upstream direction of the plasma flow through the wake,

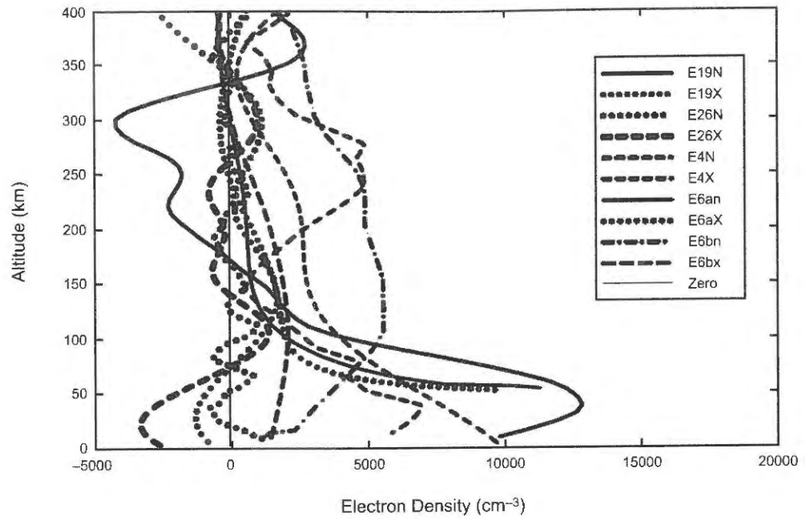

Fig. 7. See Plate 23. Compilation of all the Galileo radio occultation and near-occultation results illustrating the nonuniformity of Europa's ionosphere. Figure courtesy of A. Kliore.

where densities could well be higher. In fact, recent work by *Schilling et al.* (2008) note that the E4 flyby took an oblique trajectory through the Europa's wake. Their models show that the peak density in the wake has a small spatial extent, and produces ion densities in agreement with the plasma results of *Paterson et al.* (1999). By contrast, a broad plasma wake, such as those in the numerical results of *Kabin et al.* (1999) and *Liu et al.* (2000), cannot reproduce the *Paterson et al.* (1999) results. This reconciles the previously noted puzzling lack of higher ionospheric densities in the wake region during the E4 flyby discussed by *McGrath et al.* (2004).

The nondetection in E6aX occurred at night near the middle of the downstream wake region, and the E26 entry occultation nondetection was at high latitude in the wake region. The wake region is shielded from the preferred direction of the plasma flow, which is toward the trailing hemisphere centered at 270 W longitude, and the electron densities there might be expected to be depleted. Also, according to the plasma model of *Saur et al.* (1998), the ionosphere can become detached from the satellite in this region. However, *Kliore et al.* (2001) also conclude, on the basis of the various geometries and detections, that a necessary condition for the detection of Europa's ionosphere may be that the trailing (plasma-impacted) hemisphere is at least partially illuminated, which may indicate that solar pbotons play a significant role in ionizing the neutral atmosphere, in addition to the magnetospheric plasma electrons.

On the other hand, *Saur et al.* (1998) found that electron impact ionization alone can generate Europa's ionosphere at the electron densities measured by *Kliore et al.* (1997). Using magnetospheric plasma conditions at Europa typical of the Voyager epoch (n_e = 38 cm^{-3} and 2 cm^{-3} at T_e = 20 eV and 250 eV, respectively) the electron impact ionization rate is 1.9×10^{-6} s^{-1}, while a solar maximum photoionization rate is 6×10^{-8} s^{-1}. Given the intrinsic time constants associated with these processes (6 and 190 d, respectively, compared with a 3.6-d orbital period), the diurnally averaged solar photoionization rate would be a factor of ~2 lower, whereas electron impact ionization depends mostly on ambient magnetospheric plasma densities. In order for photoionization to be competitive with electron impact ionization, the magnetospheric electron density would have to be ~1 cm^{-3}. For the Europa radio occultations observed in Galileo orbits E4 and E6, the ambient magnetospheric ion densities were ~25 and 15 cm^{-3}, respectively (*Paterson et al.*, 1999); the corresponding electron densities would be about 50% larger. *Kurth et al.* (2001) suggested a typical torus electron density of 80 cm^{-3} at the orbit of Europa. It is therefore very difficult to understand why the existence of an ionosphere should depend on solar illumination.

In summary, while the existence of an ionosphere at Europa is well established, its origin and characteristics are still very poorly understood.

4. MINOR SPECIES, NEUTRAL CLOUDS, AND TORUS

With the exception of atomic oxygen, discussed above, detection of other minor species associated with Europa has been at distances well above the surface, where there is no overlap with detections of the primary atmospheric species O_2 (see Fig. 1). Minor species in Europa's atmosphere can

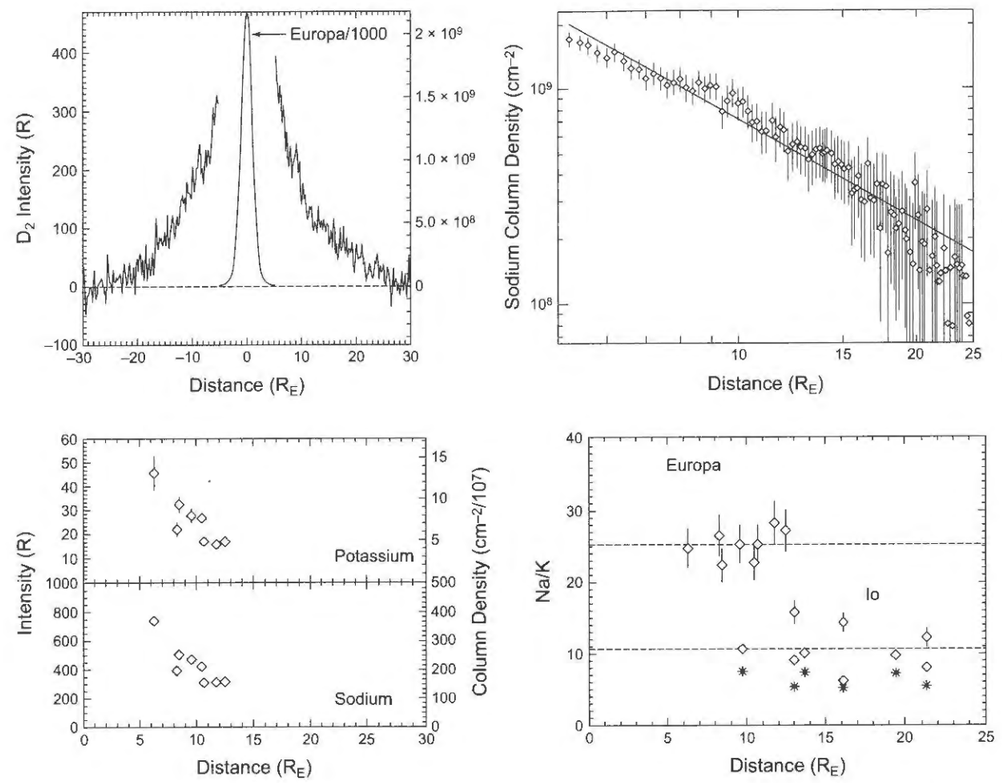

Fig. 8. *Top:* Radial profiles of Na emission from Europa obtained by *Brown and Hill* (1996). Due to a calibration error found after publication, the vertical axes in the top panel need to be multiplied by a factor of 2. *Bottom left:* Radial profiles of Na and K emission from Europa obtained by *Brown* (2001). *Bottom right:* Comparison with identical observations of Io from *Brown* (2001) shows that the Na/K ratio at Europa is about 10 times higher than that from Io. From *Brown and Hill* (1996) and *Brown* (2001).

aid in investigation of surface composition and also serve as a proxy for mapping the distribution of the major atmospheric species far from the surface. The minor species detected to date include Na, K, and some form of H (atomic or molecular). Numerous sets of observations exist of Na, Cassini made several measurements of H, but only a single set of observations has been made of K.

4.1. Sodium and Potassium

The first detection of Na from Europa was made on June 5, 1995 (observation #16 in Table 1) when 10 long-slit spectra covering 5883–5904 Å were obtained at the 1.53-m University of Arizona telescope on Mt. Bigelow with total integration time of 4.33 h (*Brown and Hill,* 1996). The long slit was oriented perpendicular to Europa's orbital plane, and emission intensity along the slit in the north-south direction from Europa was derived (top panel of Fig. 8). No variability was observed among the 10 spectra, so they were all co-added for analysis. Emission from the Na D_1 and D_2 lines at 5895.92 and 5889.95 Å, respectively, was detected with an intensity ratio of 1.70 ± 0.05, consistent with the value of 1.66 expected for optically thin emission from resonant scattering of sunlight by Na in Europa's vicinity. The line of sight column density is therefore directly proportional to the emission intensity; botb are plotted vs. radial distance in the north-south direction from Europa in Fig. 8. Note that a factor of 2 calibration error was later found in these published data, so the values along the y axes in the top panel of Fig. 8 need to be multiplied by 2. The emission is seen to be symmetric about the satellite in the north-south direction out to ~10 R_E, and then is slightly brighter in the north than the south from 10–20 R_E. The emission intensity inside ~5 R_E cannot be determined because of the overwbelming brightness of the Europa continuum. The Na emission is detectable out to ~25 R_E, which requires that Na atoms leave the surface with v > 2 km s^{-1}, and that most of the particle velocities are this large or larger to account for the flatness of the profile between 5 and 10 R_E. Since sublimation at the surface temperature of 95 K

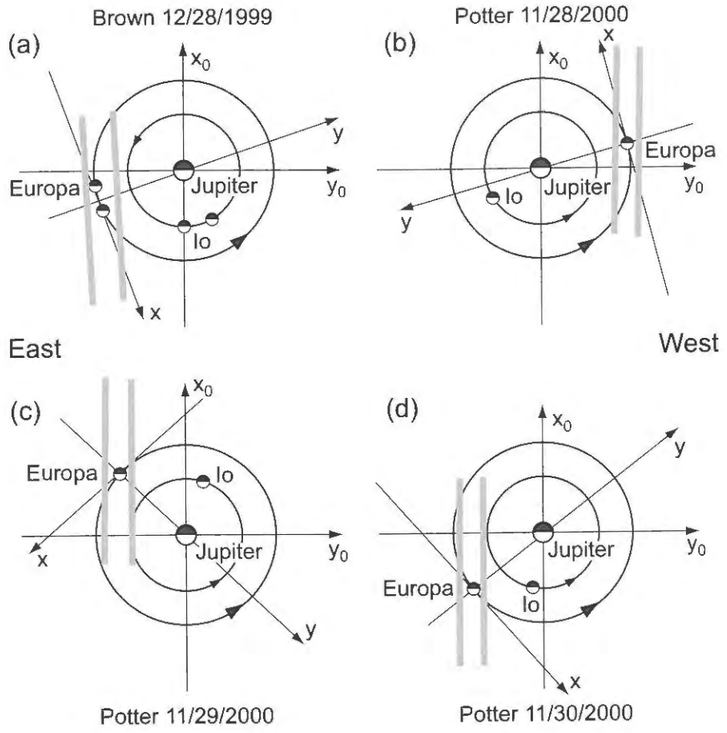

Fig. 9. Geometry of the December 1999 and November 2000 observations of Na emission near Europa reported in *Leblanc et al.* (2002, 2005). From *Leblanc et al.* (2005).

would produce velocities of only 0.3 km s^{-1}, Brown and Hill concluded that the most likely source mechanism is sputtering by energetic magnetospheric particles. The total mass of Na implied by the distribution shown in Fig. 8 is 840 kg, and extrapolation of the profile to the surface implies a surface density of ~100 cm^{-3}, which is 300 times less than the closely bound molecular oxygen atmosphere.

A second set of high-resolution, groundbased spectroscopic measurements was made on September 9, 1998, using the HIRES instrument on Keck (*Brown,* 2001). The Na observations were repeated, but this time simultaneous measurements were also made of the K doublet at 7664.90 and 7698.96 Å. The long slit was oriented perpendicular to Europa's orbital plane, and centered at several different positions east of the satellite. The intensity profile obtained (shown in the bottom panel of Fig. 8) was very similar to that from the *Brown and Hill* (1996) observations. On November 15, 1998, an identical set of observations was also made of Io. These measurements showed that the Europa Na/K ratio of ~25 is both very different from that at Io (Na/K ~ 10), and very different from a meteoritic source or the solar abundance ratios (*Brown,* 2001; *Johnson et al.,* 2002). Iogenic Na implanted into Europa's surface ice was originally suggested as the source of the Na; however, this idea was later revised based on the detection of K, and the measured ratio of Na/K for Europa compared to Io, and an endogenic source is now favored (see chapter by Johnson et al.).

Four subsequent sets of Na observations, reported in *Leblanc et al.* (2002, 2005), were obtained in 1999 by M. Brown and in 2000 by A. Potter (observations #18–21 in Table 1). The orbital geometry of Europa for these four sets of observations is shown in Fig. 9, illustrating the parts of the Na cloud observed on each occasion. The December 28, 1999, observations (reported in *Leblanc et al.,* 2002, 2005) were made with the identical setup as *Brown* (2001) using the Keck HIRES instrument, and comprised the first attempt to obtain detailed maps of the Na emission morphology near Europa. Six sets of scans were made: north-south and east-west sets centered on Europa; east-west sets at 10 R_E north and south of Europa; and east-west sets at 20 R_E north and south of Europa. The consolidated Na intensity information from these scans is shown in Fig. 10. This more complete set of measurements clearly shows that the Na cloud asymmetries are different in the direction perpendicular to the orbital plane (north-south) than in the direction parallel to the orbital plane (east-west). The observed emission morphology is again symmetric, both north-south and east-west,

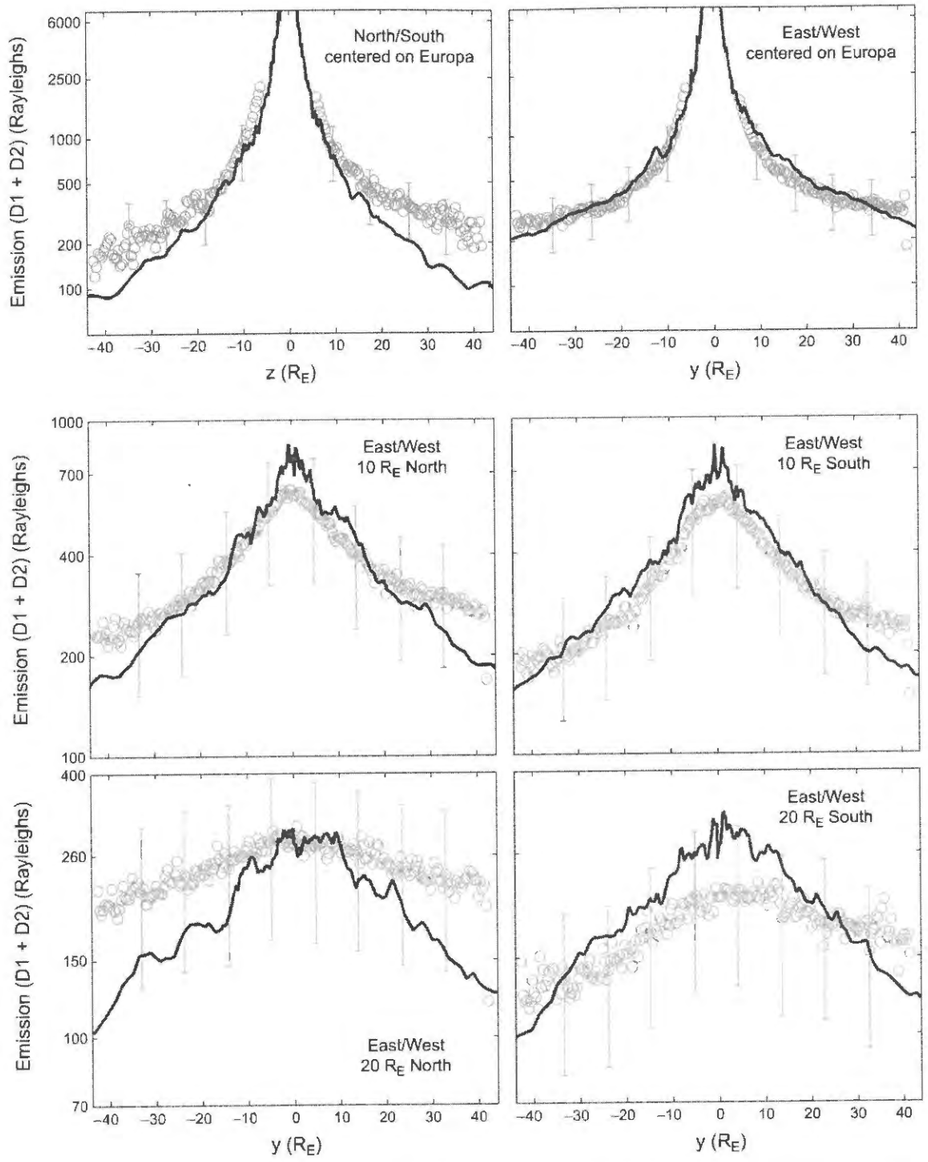

Fig. 10. Na emission profiles observed on December 28, 1999 (open circles), compared with models of *Leblanc et al.* (2002) (solid line). From *Leblanc et al.* (2002).

within ~10 R_E, but then, as with the 1995 observations, somewhat brighter north of Europa than south at d > 10 R_E. However, the overall emission intensity is approximately twice as bright in these 1999 observations than in the 1995 and 1998 observations, and substantial variations in emission intensity at given locations (e.g., 20 R_E north and south of Europa; see Fig. 10) are seen during the course of the observations.

The three sets of Na observations obtained in November 2000 used the McMath-Pierce Solar Telescope at Kitt Peak National Observatory (*Leblanc et al.,* 2005). In these observations, the Na emission was sampled in 1" × 1" regions centered at 2" and 3" from the center of Europa in all directions (north, south, east, and west) on November 28, 2000; and at 2", 3" in the north, south, east, and west directions and 4" north, east, and west on November 29 and

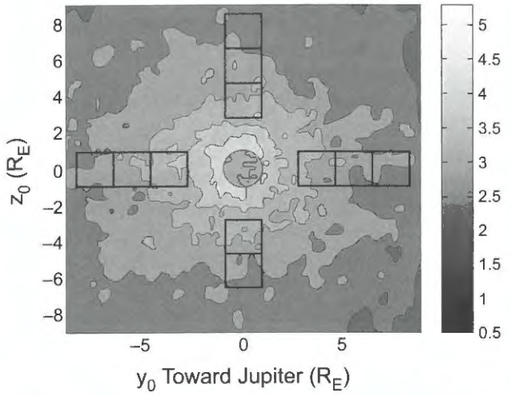

Fig. 11. Square boxes show the locations of the November 29, 2000, observations of Na near Europa superposed on a model of the Na cloud brightness of *Leblanc et al.* (2005). From *Leblanc et al.* (2005).

30, 2000. The mapping locations for the November 29 and 30, 2000, observations are illustrated in Fig. 11. Whereas earlier observations had not been obtained closer than 5 R_E, these 2000 observations obtained measurements as close as ~3.5 R_E. Table 2 of *Leblanc et al.* (2005) provides a detailed compilation of the observed Na intensities at different locations for the four sets of 1999 and 2000 observations. The differences in intensities show that within 2–3" of Europa, tbere is a leading/trailing asymmetry that *Leblanc et al.* (2005) contend is dominated by the production of atmospheric Na from the trailing hemisphere, and also depends on the solar flux. They also contend that the north-south brightness asymmetries correlate with the centrifugal (magnetic) latitude of Europa, but this is based on only a handful of data points.

A final set of (possible) Na observations add an interesting potential link between the plasma electron excited oxygen emissions and the resonant fluorescent Na emissions just described. A set of Cassini ISS clear filter images obtained on January 10, 2001, while Europa was going into eclipse (*Porco et al.,* 2003) is shown in Fig. 12. In these images, there appears to be a bright region in the northern subjovian hemisphere that persists well after Europa is completely in shadow. Porco et al. noted that Jupiter light reflected from Ganymede is a potential illumination source, but nonuniform bright emission on the Jupiter-facing hemisphere would be inconsistent with such an origin. Serendipitously, the hemisphere captured in these images is almost identical to that of the HST/STIS images shown in Figs. 4 and 5. Although the vantage point and orbital phase are very different for Cassini compared to HST, both sets of observations were viewing the trailing, plasma-bombarded hemisphere. The two sets of images both show enhancements in the northern hemisphere, but the Cassini emission is in the subjovian northern quadrant, while the HST emission is in the antijovian quadrant. Obviously, because the Cassini images were acquired while Europa was in eclipse, resonant fluorescence of sunlight is not a possible source. By analogy with similar images of Io acquired by the Galileo camera (*Geissler et al.,* 2004), *Cassidy et al.* (2008) suggested that the emission in these images may be produced predominantly by electron impact excitation of atomic Na in Europa's atmosphere. Other probable strong emitters in the ISS clear filter wavelength range include O (from O_2 dissociative excitation) and K. Cassini ISS observations were also made with a filter sensitive to O I 6300 Å emission during the same eclipse shown in Fig. 12, hut there was no signal above the noise level. The observation of O emission from Europa in eclipse [observation #8 in Table 1, described in section 2.1 above (*Retherford et al.,* 2007)] shows a somewhat similar morphology, which lends credence to the reality of the emission seen in the Cassini eclipse images. These images, along with the variation seen in the O emission morphology shown in Fig. 5, tend to support the interpretation that the various morphologies seen for both the (potentially) electron excited Na and oxygen emissions are caused by variations in the plasma and its interaction with Europa, rather tban nonuniform surface properties of the satellite or localized sputtering sources or sinks, as has been put forward by *Cassidy et al.* (2007, 2008).

4.2. Europa Torus

As Cassini approached Jupiter, the Ion and Neutral Camera (INCA), which is a channel of the Magnetospheric Imaging Instrument (MIMI), was used to acquire a 15-hr Energetic Neutral Atom (ENA) image of the Jupiter system beginning on January 1, 2001, when Cassini was at a distance of 140 R_J (Fig. 13). ENAs are produced by charge exchange between neutral atoms and magnetically trapped energetic ions. Bright features were noted in the ENA image on hoth sides of Jupiter, peaking just outside Europa's orbit at a distance of ~9.5 R_J (*Mauk et al.,* 2003). Mauk et al. interpreted their image as a torus of neutral atoms centered on the orbit of Europa. When magnetically trapped energetic protons in the Jupiter system collide with a neutral atom in such a torus, charge exchange ionizes the neutral atom and neutralizes the original proton, which then leaves the system. Tbe INCA observations cannot distinguish the composition of the original target neturals. The most likely constituents available for charge exchange in the vicinity of Europa are the products of its sputtered water ice surface and oxygen atmosphere: H_2O, H, H_2, O, OH, and O_2. The INCA data are consistent with an emission region with a radial extent and height of 1–5 R_J, symmetric about Europa's orbit, and a total content of ~9×10^{33} particles. Assuming a torus radius of 2 R_J gives a density of ~40 particles (atoms or molecules) cm^{-3}. This interpretation is corroborated by the Galileo Energetic Particle Detector (EPD) instrument measurement of a depletion of energetic particle flux in the vicinity of Europa's orbit (*Lagg et al.,* 2003).

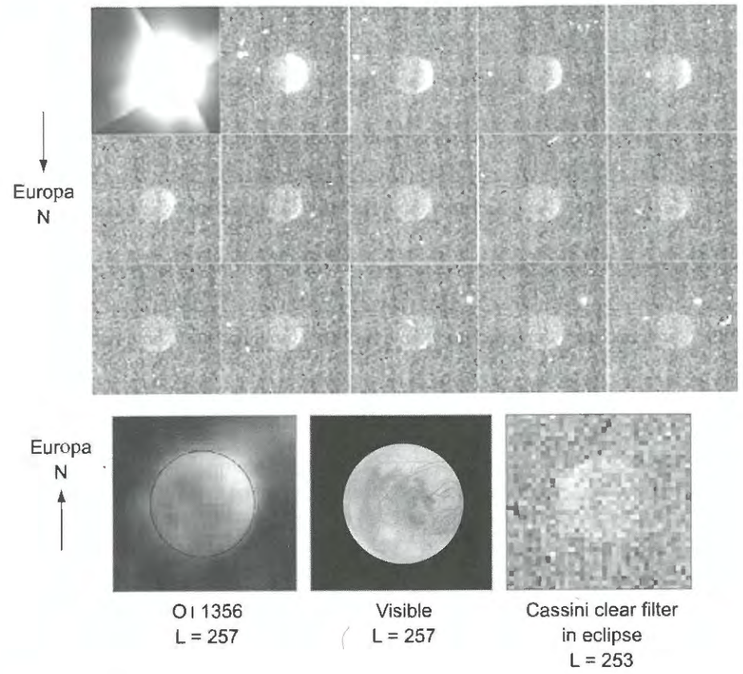

Fig. 12. Top panel shows a series of clear filter Cassini ISS camera images of Europa as it enters Jupiter's shadow, with the time sequence going from left to right, top to bottom. These observations captured the same hemisphere of Europa as the HST observations shown in Figs. 4 and 5. The 11th image from the Cassini sequence (row 3, column 1 of the top panel) is compared to both the HST O I 1356 Å emission image acquired in 1999 (same image as Fig. 4 but without brightness contours), and with a visible image of the same hemisphere of Europa. The HST and Cassini emissions are both brightest in the northern hemisphere of the satellite; however, the brightest HST emission occurs on the antijovian hemisphere, while the brightest Cassini emission occurs on the suhjovian hemisphere.

The atomic oxygen in Europa's extended atmosphere is subject to ionization and loss due to photoionization, charge exchange, and electron impact ionization. The rate of ionization from these three processes is ~1.6×10^{-6} per second, thus the lifetime for an oxygen atom in Europa's exosphere is estimated to be 7.2 d. In theory enough oxygen atoms are lost from Europa's atmosphere to account for the total number required by *Mauk et al.* (2003) as neutral species distributed in the magnetosphere. In order to put upper bounds on oxygen in the Europa torus, *Hansen et al.* (2005) analyzed data from a February 2001 outbound Cassini UVIS observation. For tbis observation the UVIS slit was centered on Jupiter and aligned parallel to Jupiter's equator (see Fig. 6a of *Hansen et al.,* 2005), and the total observation time is ~28 h. During the observation the boresight was slewed slowly from north to south every 30 min, so that the total integration time is ~7 h in any particular direction. Figure 6b of *Hansen et al.* (2005) shows a two-dimensional plot of these data. Atomic oxygen emission from the Io torus is evident, but there is no atomic oxygen emission at or near the position of Europa. If oxygen is a contributor to the torus identified by *Mauk et al.* (2003), its density must be below levels detectable by UVIS. The density that UVIS could have detected is ~8 atoms/cm^3, a factor of 5 less than the value postulated by Mauk et al. for a torus radius of 2 R_J. This suggests that the torus is substantially more extended, possibly out to the 5 R_J considered by Mauk et al., or that it is composed of H and/or H_2. Recent work by *Smyth and Marconi* (2006) argue for H_2 being the most abundant species in the Europa neutral torus (see further details in the chapter by Johnson et al.).

5. VARIABILITY

The multiple observations described above and summarized in Table 1 afford an opportunity to assess, to a limited extent, the degree of variability of Europa's atmosphere and neutral clouds. The major difficulty is our limited ability

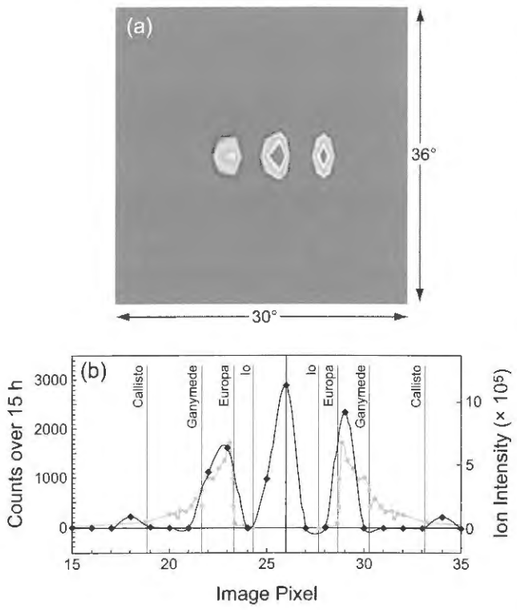

Fig. 13. **(a)** INCA image (in counts) of Jupiter and Europa from *Mauk et al.* (2003) showing an edge-on view of a torus of neutral material (most likely hydrogen) just outside the orbit of Europa. **(b)** The top two-dimensional image collapsed along the vertical axis and plotted as the black line with the intensity of protons, energy-integrated from 50 to 80 keV, plotted in the gray line. The orbits of the Galilean satellites are indicated with vertical lines. From *Mauk et al.* (2003).

to derive meaningful atmospheric neutral abundances because of our scant knowledge about the properties, including variation, of the magnetospheric plasma in the vicinity of Europa. All the observed emissions are an integral along the line of sight, and virtually all inversions of the brightness to derive column densities to date assume a uniform value for electron density and temperature. The only detailed forward modeling to date, by *Saur et al.* (1998), has not been successful in reproducing the oxygen emission morphology. It is important to bear this limitation in mind while considering what solid information can be gleaned from the observed variability.

There are nine sets of observations of the O_2 atmosphere by HST and Cassini (six with quantitative line fluxes), five sets of radio occultations of the ionosphere, and six sets of Na observations taken at different orbital, solar illumination, and magnetic geometries, including multiple observations with roughly the same orientation taken at different times. There are also two observations of the Europa torus, albeit one a nondetection. We consider each in turn.

The disk-averaged spectroscopic line fluxes for O I 1356 Å from the HST and Cassini observations (both the observed fluxes and fluxes normalized to a common distance) are given in Table 2. The observations from Table 1 have been numbered, and are referenced by number in Table 2 and in the discussion that follows. HST has observed Europa's dayside, leading hemisphere twice (observations #2 and #10), its dayside trailing hemisphere three times (observations #1, 3, and 4), and its dayside hemisphere in eclipse twice (observations #8 and 9). Disk average line fluxes are not available for observations #8, 9, and 10. Two of the trailing hemisphere observations (observations #1 and 3) were performed in an identical manner separated by a little over two years; the third trailing hemisphere observation (observation #4) was performed with a different instrument, but the line fluxes derived from it should be directly comparable to the other two. There is no significant variation in the disk-integrated O I 1356 Å line flux between observations #1 and 3, but an ~60% brightening between observations #1 and 3 and observation #4 acquired over three years after observation #3. *Hall et al.* (1995) noted that caution is warranted in interpreting the flux from observation #1 because "during the first HST orbit, the telescope was aligned so that Europa was centered in the aperture; however, during the third orbital exposure, the telescope boresight drifted ~0.8 arcsec from this initial orientation. This drift means that much of Europa's disk may have been excluded from the aperture, possibly artificially depressing detected emission intensities."

Since the oxygen atmosphere is widely accepted to be sputter generated, and the observed emissions are also excited by the plasma, the observed variability seems more likely to be caused by plasma variability than by significant changes in the surface properties of Europa that would affect the sputtering source, unless a currently undetected phenomenon such as surface geysers or surface outgassing are operative. Variability of emission morphology over a 6.5-hr interval also appears to be present in the 1999 HST observations (Fig. 5), although the low S/N ratio hampers the interpretation.

TABLE 2. Variability of O I 1356 Å flux.

Observation #*	Observed† O I 1356 Å	Normalized‡ O I 1356 Å
1	11.1 ± 1.7	0.42
2	12.9 ± 1.3	0.41
3	14.2 ± 1.5	0.45
4	24.0	0.69
Orbit 1	25.2	0.73
Orbit 2	20.6	0.59
Orbit 3	23.1	0.66
Orbit 4	28.9	0.83
Orbit 5	21.0	0.60
5	0.99	0.99
6	0.18	0.36

*Observation # from column 1 of Table 1.
†1, 2, 3, and 4 are in units of 10^{-5} photons/cm²/s; 5 and 6 are in units of photons/cm²/s.
‡In units of photons/cm²/s normalized to 6 Jan 2001 Cassini range of 11.2 × 10^6 km.

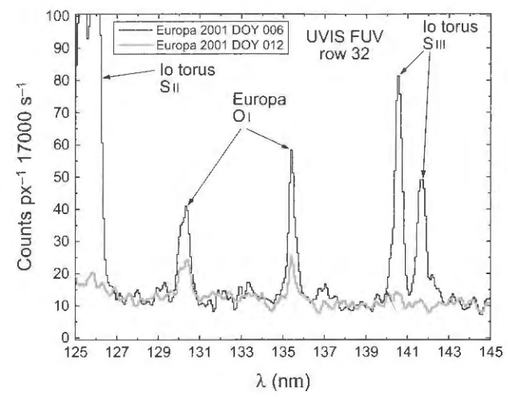

Fig. 14. Comparison of January 6 and January 12, 2001, exposures with the flux from the latter reduced by a factor of ~3. With Europa at the ansa of its orbit as seen from Cassini, Io's torus was not within the UVIS field of view on January 12. From *Hansen et al.* (2005).

The Cassini observations of Europa were at significantly different orbital locations than the HST observations, on the solar (observation #6) and roughly antisolar (observation #5) sides of Jupiter. As with the HST observations, there is a significant variation of the oxygen emission between the two Cassini observations. This is illustrated in Fig. 14, where the difference between the January 6 and January 12 datasets is clearly evident. As can be seen from Table 2, the line fluxes decreased by a factor of 3 in the 6 d between the observations. In order to explore the variability due to viewing geometry, *Hansen et al.* (2005) calculated the emission using the electron environment presented by *Saur et al.* (1998). The Saur et al. model features a steady-state distribution of electron energies around Europa, with plasma flowing in on one side and creating a cavity on the other, producing nonuniform excitation of the oxygen. At the time of the January 12 observation UVIS was looking at the leading side of Europa, at a wake region depleted of electrons. The UVIS observations are qualitatively consistent with the Saur et al. model; however, only a factor of ~1.6 difference in brightness can be attributed to the difference in leading vs. trailing side electron density and electron energy with the Saur model, vs. the 3× difference in flux observed. Using the Saur model for the spatial distribution of electrons and accounting for the viewing geometry, molecular oxygen abundances of 7.4 × 10^{14} cm^{-2} on January 12 and 12.4 × 10^{14} cm^{-2} on January 6 were calculated. The spectra show no indication of a variable O I 1356 Å intensity on January 12 over an 11.4-hr time interval (see Fig. 5 of *Hansen et al.*, 2005), which discounts an electron environment variability associated with the Io torus wobble. An increase in oxygen abundance between January 6 and January 12 might be indicative of a transient event, but the significant decrease between the two observations is harder to explain as a transient phenomenon. The more likely explanation is a change in the plasma environment, such as reported by *Frank et al.* (2002).

It is also interesting to compare the Cassini observations with the HST observations. HST observation #1 and Cassini observation #5 captured Europa at almost identical orbital phases (thus the same plasma bombardment orientation) but viewed from different directions. Cassini saw the flank of the plasma flow (30° toward the leading hemisphere), with the half toward the plasma flow being sunlit and the downstream half (with respect to the plasma flow) in darkness, while HST saw the trailing sunlit hemisphere. In this comparison, the less sunlit and less bombarded hemisphere has twice as much flux at 1356 Å. HST observation #2 and Cassini observation #6 saw the same hemisphere of the satellite at very different orbital phases. In this case, HST saw the leading (downstream) sunlit hemisphere, while Cassini saw the leading (downstream) hemisphere with half in sunlight and half in darkness; the HST 1356 Å flux is about 30% larger. It is tempting, as with the ionosphere observations, to associate higher fluxes (densities) with the presence of sunlight; however, there is so little data that this can only be characterized as an indication of a potential trend.

As mentioned briefly in section 2.1, the variation in emission morphology seen in the six consecutive HST 1356 images shown in Fig. 5, for which the sunlight, bombardment, and orbital position change very little over the course of the observations, argues fairly strongly against the emission enhancement in the antijovian hemisphere being associated with surface effects such as locally enhanced sputtering or preferential sticking in visibly dark surface regions, and in favor of variation of the plasma associated with the wobbling of the background jovian magnetic field, as has been seen at Io. However, as pointed out by *McGrath et al.* (2000) and *Ballester et al.* (2007), unlike at Io, there is not a straightforward correlation between the emission morphology and the change in background field orientation.

Finally, regarding the oxygen observations, we should note that as mentioned briefly in section 2.1, the intensity ratio of O I 1356 to O I 1304 — which is indicative of the source process (e.g., process (4) or (5), outlined in section 2.1, or both) — appears to exhibit significant variability. *Hall et al.* (1998) found a range of 1–2, yet argued that this was consistent with no measureable atomic oxygen in all cases. *Hansen et al.* (2005) find a ratio of 1.8–2.1, but argue for the detectable presence of atomic oxygen in the bound atmosphere. Even the higher value of ~2 is only at best marginally consistent with the best available cross-section data and our knowledge of the electron temperature near Europa. It may indeed be the case that variability of the atomic emission line intensities is indicative of variations in both O_2 and O abundances, and variation in the abundance of one relative to the other.

The ionosphere observations show a range of levels of detection, including two nondetections, the E6a exit (observation #12) and the E26 entry (observation #15). It's

TABLE 3. Summary of Europa's atmosphere, neutral clouds, and torus.

Species	Density	Location	Reference
O_2	(2.4–14) × 10^{14} cm^{-2}	line of sight	1,2,3
	(3.7–6.2) × 10^7 cm^{-3}	mean (H = 200 km)	2
	(5–10) × 10^9 cm^{-3}	surface	4,5
O	(1.7–3.1) × 10^{13} cm^{-2}	line of sight	2
	(0.85–1.5) × 10^6 cm^{-3}	mean (H = 200 km)	2
	1000–1700 cm^{-3}	<22,000 km	this work
	few × 10^4 cm^{-3}	surface	4,5
O/O_2	<0.1	H ~ 20–300 km	1
	~0.02	H = 200 km	2
n_e (ionosphere)	peak ~ 10^3–10^4 cm^{-3}	<300 km	6
Na	(4–0.4) × 10^9 cm^{-2}	5–25 R_E	7,8
	~100 cm^{-3}	surface	7,8
K	~0.04 × Na	5–13 R_E	8
Na/K	25	5–13 R_E	8
H or H_2 torus	~40 cm^{-3}	r ~ 2 R_J?	9
O torus	<8 cm^{-3}	if r ~ 2 R_J	2

References: [1] *Hall et al.* (1998); [2] *Hansen et al.* (2005); [3] *Saur et al.* (1998); [4] *Shematovich et al.* (2005); [5] *Smyth and Marconi* (2006); [6] *Kliore et al.* (1997, 2006); [7] *Brown and Hill* (1996); [8] *Brown* (2001); [9] *Mauk et al.* (2003).

interesting to note that the E4 ionosphere occultation occurred for a Europa geometry (orbital, sunlight, plasma bombardment) that is nearly identical to that for HST observation #4 (shown in Figs. 4 and 5), except Galileo is looking toward the upstream direction, while HST is looking toward the downstream direction. This is the HST observation that shows the brightest 1356 Å emission region in the antijovian hemisphere, which corresponds to the E4 exit measurement that shows a very weak, low-scale height electron density profile. The geometry (orbital, sunlight, plasma bombardment) for the E6a radio occultation is nearly identical to Cassini observation #6. The E6a entry profile is along the ram direction, which may explain the compressed, low-scale height nature of this profile, whereas the E6a exit profile is along the middle of the wake, and is a nondetection. This Cassini observation corresponds to an oxygen density at the low end of the range observed in the six sets of observations. Finally, the E6b exit profile is over the longitude (256°W) at the center of the HST observation #4 images shown in Fig. 4, where there is no obvious 1356 Å emission.

The variations seen in the Na observations are complex, and have been explored in detail in *Leblanc et al.* (2005). One interesting conclusion they draw is that the total emission intensity from one measurement to another cannot be explained solely by the differences in the geometry of the observations, and it is likely that there was a significant variation in the source rate from November 28, 2000, to November 30, 2000. This is a rich dataset that is continuing to be exploited with ongoing investigations and modeling (e.g., *Cipriani et al.,* 2008). The current thinking concerning the variations seen closest to the satellite is described further in the chapter by Johnson et al. (see their Fig. 2).

6. SUMMARY: OUTSTANDING ISSUES AND FUTURE WORK

We summarize in Table 3 our current knowledge of Europa's tenuous atmosphere, neutral clouds, and torus. Although substantial progress has been made in characterizing them in the past 14 years since the first detection of oxygen emission, the data continues to be very sparse. We have only a rudimentary understanding of the source(s) and sinks for the atmosphere; in particular, it is unclear if localized sources such as geysers are present. A better understanding may come only when additional atmospheric species, such as OH, H_2, H_2O, CO, or CO_2, are detected. For instance, a substantial although transient H_2O sublimation atmosphere will be present in the equatorial regions when the subsolar point is over the icy leading hemisphere but may be absent when the subsolar point is over the trailing hemisphere, which is likely dominated by water of hydration. Such variability will affect the ionosphere. Since the surface materials are decomposed by radiolysis a large number of products other than O_2 and H_2 should be present, like the Na and K components discussed above. Carbon dioxide has been detected in the surface ice (*Smythe et al.,* 1998) and appears to be correlated with the dark terrain on the antijovian and leading hemispheres (*Hansen and McCord,* 2008). Although the CO_2 band depth is comparable to that measured at Callisto, no measurement of CO_2 in vapor form has been made at Europa. *Hansen and McCord* (2008) suggest an internal, subsurface ocean source for the surface CO_2. Searches for CO_2 and its products (CO, C) should be performed at Europa in future. Given that the CO_2 atmosphere on Callisto has not been detected from Earth, detections may be difficult to accomplish by remote sensing. Techniques such as those currently being used on Cassini (including mass spectrometers, stellar occultations, and detailed plasma characterization), as well as high-resolution IR spectroscopy for identification of surface constituents, would be useful tools on future missions to Europa or the jovian system.

Interpretation of the observations is also hampered by the lack of understanding of the local plasma environment, and its variability, at Europa. Further *in situ* characterization is critical because, unlike Io, the plasma near Europa is too tenuous to be observed with current groundbased and Earth-orbit techniques. Until further data are obtained, continued work on detailed interaction models such as those of *Saur et al.* (1998) and *Shilling et al.* (2008) are indispensible in trying to make further progress interpreting the data already in hand.

There is also additional worthwhile work to be done on the existing data. For example, all the GHRS spectra acquired by HST contain temporal information that has yet to be exploited. Upper limits for CO and CO_2 abundances could be estimated from the HST spectra, as has been done for Callisto (*Strobel et al.,* 2002). The HST STIS is scheduled to be repaired during Servicing Mission 4 in 2009. Further observations of the oxygen emissions such as those shown in Figs. 4 and 5 would be very useful. It would be helpful if HST and/or groundbased observations could be done to confirm and/or extend the Cassini eclipse images shown in Fig. 12.

Perhaps the best immediate route for progress is groundbased observing programs aimed at characterizing the Na and K clouds at Europa. Such observations are clearly feasible, and until further observations of the main constituents are obtained, Na and K serve as very useful proxies for understanding the surface/plasma source and loss processes operative at Europa.

Acknowledgments. We would like to sincerely thank A. Campbell for providing Figs. 4 and 5; K. Retherford for sharing results prior to publication; and P. Geissler and A. Kliore for sharing details about their Europa research. The research described in this chapter carried out at the Jet Propulsion Laboratory, California Institute of Technology, was done so under a contract with the National Aeronautics and Space Administration.

REFERENCES

Ballester G. E., Herbert F., Kivelson M., Khurana K. K., and Combi M. R. (2007) Studies of Europa's plasma interactions and atmosphere with HST/STIS far-UV images (abstract). In *Magnetospheres of the Outer Planets,* p. 98. Southwest Research Institute, San Antonio.

Barth C. A., Hord C. W., Stewart A. I. F., Pryor W. R., Simmons K. E., McClintock W. E., Ajello J. M., Naviaux K. L., and Aiello J. J. (1997) Galileo ultraviolet spectrometer observations of atomic hydrogen in the atmosphere at Ganymede. *Geophys. Res. Lett., 24,* 2147–2150.

Broadfoot A. L., Belton M. J., Takacs P. Z., Sandel B. R., Shemansky D. E., Holberg J. B., Ajello J. M., Moos H. W., Atreya S. K., Donahue T. M., Bertaux J. L., Blamont J. E., Strobel D. F., McConnell J. C., Goody R., Dalgarno A., and McElroy M. B. (1979) Extreme ultraviolet observations from Voyager 1 encounter with Jupiter. *Science, 204,* 979–982.

Brown M. E. (2001) Potassium in Europa's atmosphere. *Icarus, 151,* 190–195.

Brown M. E. and Hill R. E. (1996) Discovery of an extended sodium atmosphere around Europa. *Nature, 380,* 229–231.

Brown R. A. (1974) Optical line emission from Io. In *Exploration of the Planetary System* (A. Woszczyk and C. Iwaniszewska, eds.), pp. 527–531. IAU Symposium 65, Reidel, Dordrecht.

Brown W. L., Augustyniak W. M., Lanzerotti L. J., Poate J. M., and Augustyniak W. M. (1977) *Eos Trans. AGU, 58,* 423.

Brown W. L., Augustyniak W. M., Lanzerotti L. J., Johnson R. E., and Evatt R. (1980) Linear and nonlinear processes in the erosion of H_2O ice by fast light ions. *Phys. Rev. Lett., 45,* 1632–1635.

Burger M. H. and Johnson R. E. (2004) Europa's neutral cloud: Morphology and comparisons to Io. *Icarus, 171,* 557–560.

Carlson R. W., Bhattacharyya J. C., Smith B. A., Johnson T. V., Hidayat B., Smith S. A., Taylor G. E., O'Leary B., and Brinkmann R. T. (1973) An atmosphere on Ganymede from its occultation of SAO 186800 on 7 June 1972. *Science, 182,* 53–55.

Cassidy T. A., Johnson R. E., McGrath M. A., Wong M. A., and Cooper J. F. (2007) The spatial morphology of Europa's near-surface O_2 atmosphere. *Icarus, 191,* 755–764.

Cassidy T. A., Johnson R. E., Geissler P. E., and Leblanc F. (2008) Simulation of Na D emission near Europa during eclipse. *J. Geophys. Res., 113,* E02005.

Cipriani F., Leblanc F., and Witasse O. (2008) Sodium recycling at Europa: What do we learn from the sodium cloud variability? *Geophys. Res. Lett., 35,* L19201, DOI: 10.10292008GR035061.

Doering J. P. and Yang J. (2001) Atomic oxygen ^3P–$^3S^o$ (λ1304 Å) transition revisited: Cross section near threshold. *J. Geophys. Res., 206,* 203–210.

Feldman P. D., McGrath M. A., Strobel D. F., Moos H. W., Retherford K. D., and Wolven B. C. (2000) HST/STIS ultraviolet imaging of polar aurora on Ganymede. *Astrophys. J., 535,* 1085–1090.

Frank L. A., Ackerson K. L., Wolfe J. H., and Mihalov J. D. (1976) Observations of plasmas in the jovian magnetosphere. *J. Geo-phys. Res., 81,* 457.

Frank L. A., Paterson W. R., and Khurana K. K. (2002) Observations of thermal plasmas in Jupiter's magnetotail. *J. Geophys. Res., 107(A1),* DOI: 10.1029/2001JA000077.

Geissler P., McEwen A., Porco C., Strobel D., Saur J., Ajello J., and West R. (2004) Cassini observations of Io's visible aurorae. *Icarus, 172,* 127–140.

Hall D. T., Strobel D. F., Feldman P. D., McGrath M. A., and Weaver H. A. (1995) Detection of an oxygen atmosphere on Jupiter's moon Europa. *Nature, 373,* 677–679.

Hall D. T., Feldman P. D., McGrath M. A., and Strobel D. F. (1998) The far-ultraviolet oxygen airglow of Europa and Ganymede. *Astrophys. J., 499,* 475–481.

Hansen C. J., Shemansky D., and Hendrix A. (2005) Cassini UVIS Observations of Europa's oxygen atmosphere and torus. *Icarus, 176,* 305–315.

Hansen G. B. and McCord T. B. (2008) Widespread CO_2 and other non-ice compounds on the anti-jovian and trailing sides of Europa from Galileo/NIMS observations. *Geophys. Res. Lett., 35,* L01202.

Hendrix A. R. and Hansen C. J. (2008) Ultraviolet observations of Phoebe from the Cassini UVIS. *Icarus, 193,* 323–333.

Johnson R. E. (2002) Surface boundary layer atmospheres. In *Atmospheres in the Solar System: Comparative Aeronomy* (M. Mendillo et al., eds.), pp. 203–219. AGU Geophysical Monograph 130, Washington, DC.

Johnson R. E., Lanzerotti L. J., and Brown W. L. (1982) Planetary applications of ion induced erosion of condensed gas frosts. *Nucl. Instr. Meth.Phys. Res., A198,* 147–158.

Johnson R. E., Leblanc F., Yakshinskiy B. V., and Madey T. E. (2002) Energy distributions for desorption of sodium and potassium from ice: The Na/K ratio at Europa. *Icarus, 156,* 136–142.

Judge D. L. and Carlson R. W. (1974) Pioneer 10 observations of the ultraviolet glow in the vicinity of Jupiter. *Science, 183,* 317.

Judge D. L., Carlson R. W., Wu F.-M., and Hartmann U. G. (1976) Pioneer 10 and 11 ultraviolet photometer observations of the jovian satellites. In *Jupiter* (T. Gehrels et al., eds.), p. 1068. Univ. of Arizona, Tucson.

Kabin K., Combi M. R., Gombosi T. I., Nagy A. F., DeZeeuw D. L., and Powell K. G. (1999) On Europa's magnetospheric interaction: A MHD simulation of the E4 flyby. *J. Geophys. Res., 104(A9),* 19983–19992.

Kanik I., Noren C., Makarov O. P., Vattipalle P., and Ajello J. M. (2003) Electron impact dissociative excitation of O_2: 2. Absolute emission cross sections of the O I (130.4 nm) and O I (135.6 nm) lines. *J. Geophys. Res., 108,* 5126, DOI: 10.1029/2000JE001423.

Kivelson M. G., Khurana K. K., Coroniti F. V., Joy S., Russell C. T., Walker R. J., Warnecke J., Bennett L., and Polanskey C. (1997) Magnetic field and magnetosphere of Ganymede. *Geo-phys. Res. Lett., 24,* 2155.

Kliore A., Cain D. L., Fjeldbo G., Seidel B. L., and Rasool S. I. (1974) Preliminary results on the atmospheres of Io and Jupiter from the Pioneer 10 S-band occultation experiment. *Science, 183,* 323–324.

Kliore A. J., Fjeldho G., Seidel B. L., Sweetnam D. N., Sesplaukis T. T., Woiceshyn P. M., and Rasool S. I. (1975) The atmosphere of Io from Pioneer 10 radio occultation measurements. *Icarus, 24,* 407–410.

Kliore A. J., Hinson D. P., Flasar F. M., Nagy A. F., and Cravens T. E. (1997) The ionosphere of Europa from Galileo radio occultations. *Science, 277,* 355–358.

Kliore A. J., Anabtawi A., and Nagy A. F. (2001) The ionospheres of Europa, Ganymede, and Callisto. *Eos Trans. AGU, 82(47),* Fall Meet. Suppl., Abstract #P12B-0506.

Kliore A. J., Nagy A. F., Flasar F. M., Schinder P. J., and Hinson D. P. (2006) Radio science data on the ionospheres of Jupiter, Saturn, and their major satellites. *36th COSPAR Scientific Assembly,* Beijing, China, Abstract #2599.

Kumar S. (1982) Photochemistry of SO_2 in the atmosphere of Io and implications on atmospheric escape. *J. Geophys. Res., 87,* 1677–1684.

Kupo I., Mekler Y., and Eviatar A. (1976) Detection of ionized sulfur in the jovian magnetosphere. *Astrophys. J. Lett., 205,* L51–L53.

Kurth W. S., Gurnett D. A., Persoon A. M., Roux A., Bolton S. J., and Alexander C. J. (2001) The plasma wave environment of Europa. *Planet. Space Sci., 49,* 345–363.

Lagg A, Krupp N., Woch J., and Williams D. J. (2003). In-situ observations of a neutral gas torus at Europa. *Geophys. Res. Lett., 30,* DOI: 10.1029/2003GL017214.1556.

Lanzerotti L. J., Brown W. L., Poate J. M., and Augustyniak W. M. (1978) On the contribution of water products from Galilean satellites to the jovian magnetosphere. *Geophys. Res. Lett., 5,* 155–158.

Leblanc F., Johnson R. E., and Brown M. E. (2002) Europa's sodium atmosphere: An ocean source? *Icarus, 159,* 132.

Leblanc F., Potter A. E., Killen R. M., and Johnson R. E. (2005) Origins of Europa Na cloud and torus. *Icarus, 178,* 367–385.

Liu Y., Nagy A. F., Kabin K., Comhi M. R., Dezeeuw D. L., Gombosi T. I., and Powell K. G. (2000) Two-species, 3D, MHD simulation of Europa's interaction with Jupiter's magnetosphere. *Geophys. Res. Lett., 27(12),* 1791–1794.

Mauk B. H., Mitchell D. G., Krimigis S. M., Roelof E. C., and Paranicas C. P. (2003) Energetic neutral atoms from a trans-Europa gas torus at Jupiter. *Nature, 421,* 920–922.

McDonough T. R. and Brice N. M. (1973) A saturnian gas ring and the recycling of Titan's atmosphere. *Icarus, 20,* 136.

McGrath M. A., Feldman P. D., Strobel D. F., Retherford K., Wolven B., and Moos H. W. (2000) HST/STIS ultraviolet imaging of Europa. *Bull. Am. Astron. Soc., 32,* 1056.

McGrath M. A., Lellouch E., Strobel D. F., Feldman P. D., and Johnson R. E. (2004) Satellite atmospheres. In *Jupiter: The Planet, Satellites and Magnetosphere* (F. Bagenal et al., eds.), pp. 457–483. Cambridge Univ., Cambridge.

Ness N. F., Acuna M. H., Lepping R. P., Burlaga L. F., Behannon K. W., and Neubauer F. M. (1979) Magnetic field studies at Jupiter by Voyager 1 — Preliminary results. *Science, 204,* 982–987.

Neubauer F. M. (1980) Nonlinear standing Alfven wave current system at Io — Theory. *J. Geophys. Res., 85,* 1171–1178.

Noren C., Kanik I., Ajello J. M., McCartney P., Makarov O. P., McClintock W. E., and Drake V. A. (2001) Emission cross section of O I (135.6 nm) at 100 eV resulting from electron-impact dissociative excitation of O_2. *Geophys. Res. Lett., 28,* 1379+.

Paterson W. R., Frank L. A., and Ackerson K. L. (1999) Galileo plasma observations at Europa: Ion energy spectra and moments. *J. Geophys. Res., 104,* 22779–22792.

Pilcher C. B., Ridgway S. T., and McCord T. B. (1972) Galilean satellites: Identification of water frost. *Science, 178,* 1087–1089.

Porco C. and 23 colleagues (2003) Cassini imaging of Jupiter's atmosphere, satellites, and rings. *Science, 299,* 1541.

Retherford K. D., Spencer J. R., Gladstone G. R., Stern S. A., Saur J., Strobel D. F., Slater D. C., Steffl A. J., Parker J. W., Versteeg M., Davis M. W., Throop H., and Young L. A. (2007) Icy Galilean satellite UV observations by New Horizons and HST. *Eos Trans. AGU, 88(52),* Fall Meet. Suppl., Abstract #P53C-06.

Saur J., Strobel D. F., and Neubauer F. M. (1998) Interaction of the jovian magnetosphere with Europa: Constraints on the neutral atmosphere. *J. Geophys. Res., 103,* 19947–19962.

Schilling N., Neubauer F. M., and Saur J. (2008) Influence of the internally induced magnetic field on the plasma interaction of Europa. *J. Geophys. Res., 113,* A03203, DOI: 10.1029/2007JA012842.

Shematovich V. I. and Johnson R. E. (2001) Near-surface oxygen atmosphere at Europa. *Adv. Space Res., 27,* 1881–1888.

Shematovich V. I., Johnson R. E., Cooper J. F., and Wong M. C. (2005) Surface-bounded atmosphere of Europa. *Icarus, 173,* 480–498.

Smyth W. H. and Marconi M. L. (2006) Europa's atmosphere, gas tori, and magnetospheric implications. *Icarus, 181,* 510–526.

Smythe W. D., Carlson R. W., Ocampo A., Matson D. L., McCord T. B., and the NIMS Team (1998) Galileo NIMS measurements of the absorption bands at 4.03 and 4.25 microns in distant observations of Europa. *Bull. Am. Astron. Soc., 30,* Abstract #55P.07.

Strobel D. F., Saur J., Feldman P. D., and McGrath M. A. (2002) Hubble Space Telescope imaging spectrograph search for an atmosphere on Callisto: A jovian unipolar inductor. *Astrophys. J. Lett., 581,* L51–L54.

Trafton L. (1975). Detection of a potassium cloud near Io. *Nature, 258,* 690–692.

Wu F.-M., Judge D. L., and Carlson R. W. (1978) Europa: Ultraviolet emissions and the possibility of atomic oxygen and hydrogen clouds. *Astrophys. J., 225,* 325–334.

Yung Y. L. and McElroy M. B. (1977) Stability of an oxygen atmosphere on Ganymede. *Icarus, 30,* 97–103.

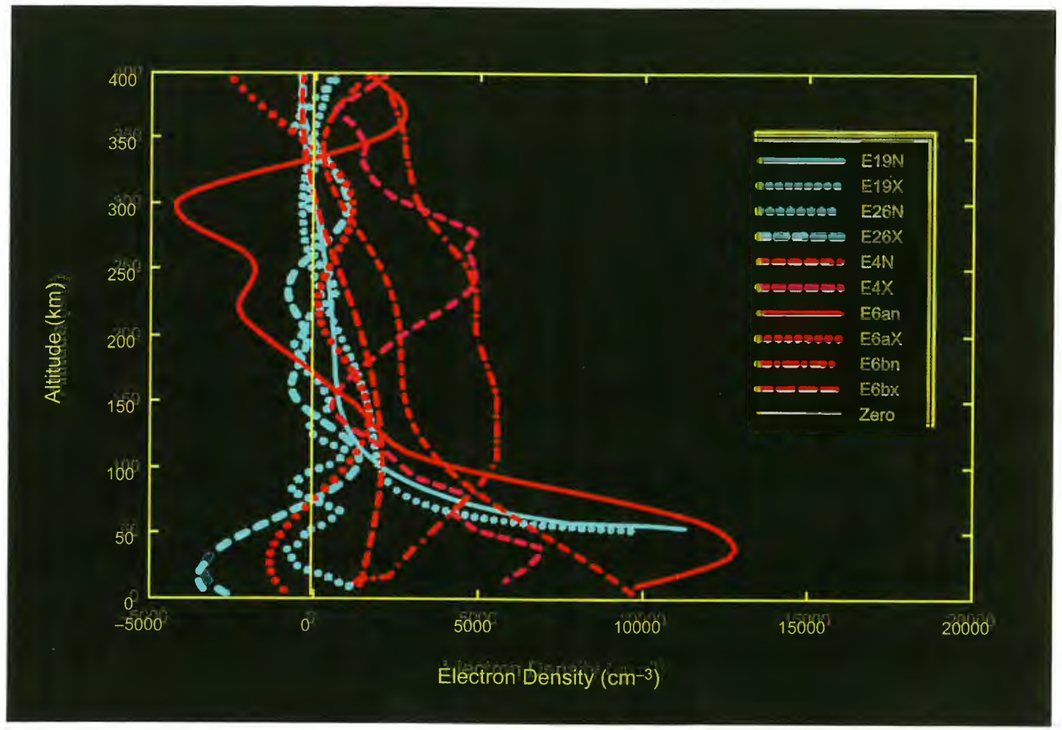

Plate 23. Compilation of all the Galileo radio occultation and near-occultation results illustrating the nonuniformity of Europa's ionosphere. Figure courtesy of A. Kliore.

Accompanies chapter by McGrath et al. (pp. 485–505).

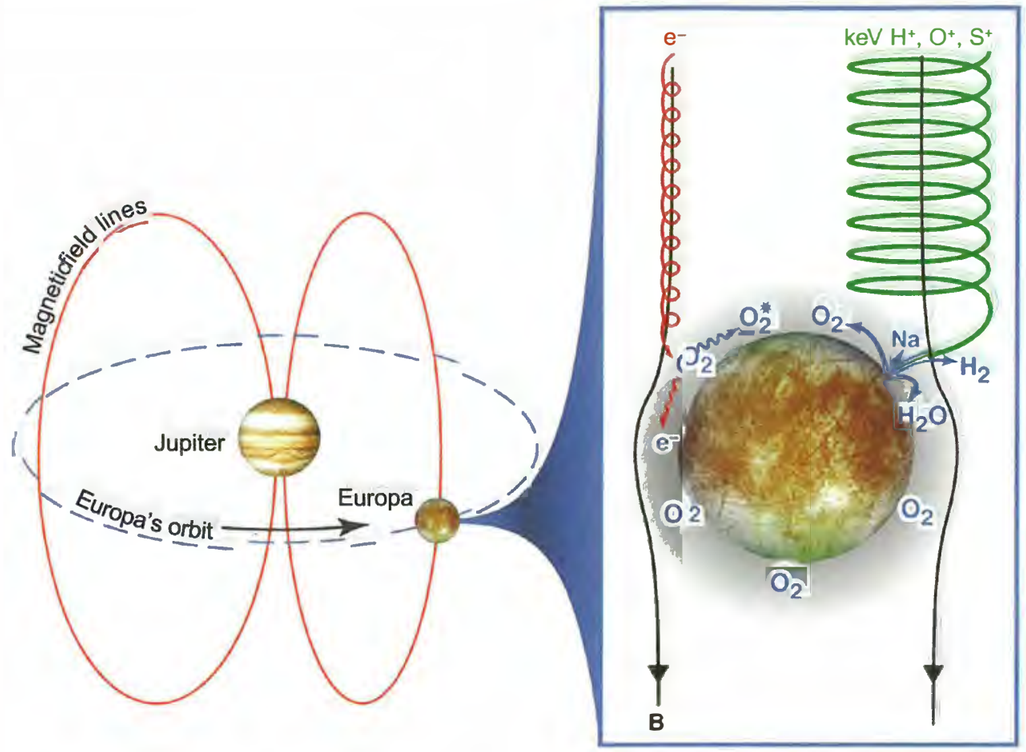

Plate 24. Schematic of Europa's interaction with Jupiter's magnetosphere. Ions and electrons trapped by Jupiter's magnetic field alter and erode the surface, producing a tenuous atmosphere composed mostly of O_2 with an extended neutral torus of primarily H_2.

Accompanies chapter by Johnson et al. (pp. 507–527).

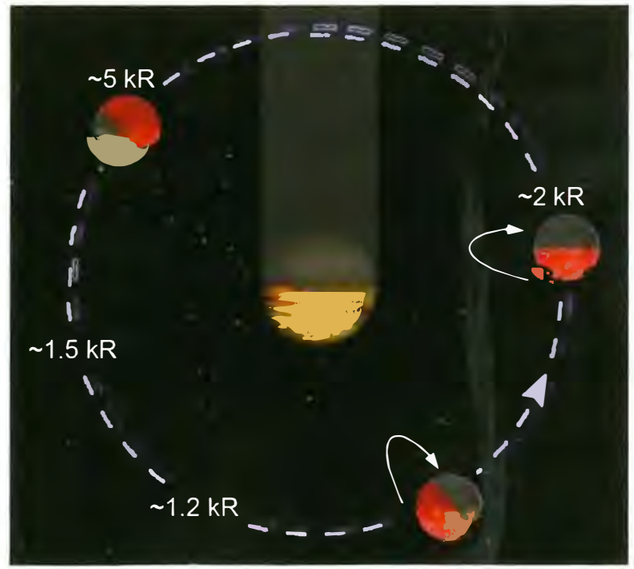

Plate 25. Average Na emission intensity (in kiloRayleigh) at 4 Europa radii from the surface at different positions around Jupiter (*Leblanc et al.*, 2005). The red part on the surface is the preferentially bombarded trailing hemisphere, whereas the dark part represents the night hemisphere. Also indicated is Jupiter's shadow at Europa's orbit; sizes of Jupiter and Europa are not to scale. White arrows indicate where accumulation of Na atoms on the leading side may occur.

Accompanies chapter by Johnson et al. (pp. 507–527).